ADVANCED ENERGY MATERIALS

Postfach 10 11 61
69451 Weinheim
Germany
Courier services:
Boschstraße 12
69469 Weinheim
Germany
Tel.: (+49) 6201 606 531
Fax: (+49) 6201 606 500
E-mail: advenergymat@wiley.com

WILEY-VCH

Dear Author,

Please correct your galley proofs carefully and return them no more than four days after the page proofs have been received.

Please limit corrections to errors already in the text; cost incurred for any further changes or additions will be charged to the author, unless such changes have been agreed upon by the editor.

The editors reserve the right to publish your article without your corrections if the proofs do not arrive in time.

Note that the author is liable for damages arising from incorrect statements, including misprints.

Please note any queries that require your attention. These are indicated with a Q in the PDF and a question at the end of the document.

Reprints may be ordered by filling out the accompanying form.

Return the reprint order form by fax or by e-mail with the corrected proofs, to Wiley-VCH : advenergymat@wiley.com

To avoid commonly occurring errors, **please ensure that the following important items are correct** in your proofs (please note that once your article is published online, no further corrections can be made):

- **Names** of all authors present and spelled correctly
- **Titles** of authors correct (Prof. or Dr. only: please note, Prof. Dr. is not used in the journals)
- **Addresses** and **postcodes** correct
- **E-mail address** of corresponding author correct (current email address)
- **Funding bodies** included and grant numbers accurate
- **Title** of article OK
- All **figures** included
- **Equations** correct (symbols and sub/superscripts)

Corrections should be made directly in the PDF file using the PDF annotation tools. If you have questions about this, please contact the editorial office. The corrected PDF and any accompanying files should be uploaded to the journal's Editorial Manager site.

Author Query Form

WILEY

Journal AENM

Article aenm202002523

Dear Author,

During the copyediting of your manuscript the following queries arose.

Please refer to the query reference callout numbers in the page proofs and respond to each by marking the necessary comments using the PDF annotation tools.

Please remember illegible or unclear comments and corrections may delay publication.

Many thanks for your assistance.

Query No.	Description	Remarks
Q-license	Please note that the article can only be published once an appropriate license agreement has been signed. The responsible corresponding author will have received an e-mail invitation to register/log in and sign a license agreement in Wiley Author Services (https://authorservices.wiley.com). The costs of publishing this manuscript OnlineOpen might be covered by one of Wiley's national agreements. To find out more please visit, https://authorservices.wiley.com/authorresources/Journal-Authors/open-access/affiliation-policies-payments/index.html. Eligibility for fee coverage is determined by the affiliation of the responsible corresponding author.	
Q1	Please confirm that forenames/given names (blue) and surnames/family names (vermilion) have been identified correctly.	
Q2	Please provide the highest academic title (either Dr. or Prof.) for all authors, where applicable.	
Q3	Please confirm that all elements of the TOC image are original, i.e., have not been published before or are sourced from online image libraries. Unoriginal work in the TOC is not permitted, as attribution information cannot be provided.	
Q4	Please define all acronyms at their first appearance in the abstract, text and table of contents, respectively. Only expanded forms are allowed if the elements are cited only once in the article.	
Q5	Please note that for all figures, elements therein, tables, and schemes that are not original to your article, permission for reproduction needs to be obtained. Please confirm that all mentioned elements in your article are either original, i.e., have not been published before, or permission for reproduction was obtained. Please cite all elements for which permission for reproduction was obtained in the following way: Reproduced (Adapted) with permission.[Ref.] Copyright Year, Publisher.	

Please confirm that Funding Information has been identified correctly.

Please confirm that the funding sponsor list below was correctly extracted from your article: that it includes all funders and that the text has been matched to the correct FundRef Registry organization names. If a name was not found in the FundRef registry, it may not be the canonical name form, it may be a program name rather than an organization name, or it may be an organization not yet included in FundRef Registry. If you know of another name form or a parent organization name for a "not found" item on this list below, please share that information.

FundRef Name	FundRef Organization Name
Key Research and Development Program of Hubei	
Australian Research Council	Australian Research Council

Q. Yu, Z. Xue, M. Li, P. Qiu, C. Li, S. Wang,* J. Yu,* H. Nara, J. Na, Y. Yamauchi* 2002523

Electrochemical Activity of Nitrogen-Containing Groups in Organic Electrode Materials and Related Improvement Strategies

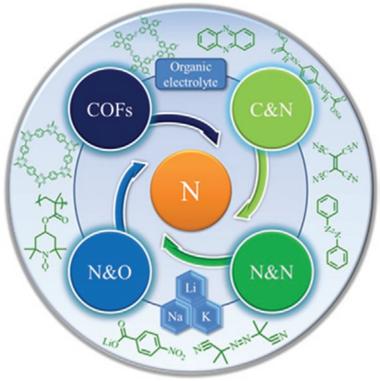

The organic compounds with nitrogen-containing groups (OCNs) have gained increasing attention as next-generation energy storage materials. This timely review summarizes the recent advances in this fast-growing field, with particular focuses on the electrochemical reaction mechanism and kinetics of the active OCNs (sites) and structure-property relationships. New strategies are proposed further to improve their insolubility, conductivity, and electrochemical performance. Q3

ADVANCED ENERGY MATERIALS
www.advenergymat.de

Electrochemical Activity of Nitrogen-Containing Groups in Organic Electrode Materials and Related Improvement Strategies

Q1
Qianchuan Yu, Zhihuan Xue, Meichen Li, Peimeng Qiu, Changgang Li, Shengping Wang,* Jingxian Yu,* Hiroki Nara, Jongbeom Na, and Yusuke Yamauchi*

In recent years, due to their structural diversity, adjustability, versatility, and excellent electrochemical properties, organic compounds with nitrogen-containing groups (OCNs) have become some of the most promising organic electrode materials. The nitrogen-containing groups acting as electrochemical active sites include carbon–nitrogen groups, nitrogen–nitrogen groups, nitrogen–oxygen groups in OCNs, and nitrogen-containing groups in covalent organic frameworks. The molecular structure regulation of OCNs with nitrogen-containing groups acting as electrochemical active centers can suppress dissolution in electrolytes, increase electronic conductivity, and improve the kinetics of redox reactions. The kinetics behavior and electrochemical characteristics of OCN electrode materials in alkali metal rechargeable batteries with organic electrolytes are reviewed, and the related relationships between the structure and electrochemical properties of OCNs are the core of this paper. Herein, the electrochemical reaction mechanisms and the strategies to improve the electrochemical activity of nitrogen-containing groups in OCNs are clarified, and the conjugate molecular structure of OCNs is an important direction for improvement. These results will have implications for research on electrode materials and provide more choices for rechargeable batteries. Moreover, this work will guide the study of more efficient OCNs that can be used as electrode materials.

1. Introduction

With the increasing demand for sustainable energy and the development of smart grids and electric vehicles, rechargeable batteries offer excellent performance and can be used for further innovation.[1–5] Regarding rechargeable batteries, although lithium-ion batteries (LIBs) have made great achievements in portable devices, such as laptops and smartphones, emerging fields of the past 20 years, such as artificial intelligence and the Internet of Things, strongly rely on smart power.[6–11] To reduce costs, sodium-ion batteries (NIBs) and potassium-ion batteries (KIBs), which have chemical properties and charge/discharge mechanisms similar to those of LIBs, have also been studied extensively.[12–14] However, the further development of rechargeable batteries has been restricted, since inorganic transition metal oxides used as electrode materials are limited and not environmentally friendly.[15–18] The solution to these problems is to replace transition metal oxides with organic materials. Organic

Q2
Q. Yu, Z. Xue, M. Li, P. Qiu, C. Li, S. Wang
Faculty of Materials Science and Chemistry
China University of Geosciences
Wuhan 430074, China
E-mail: spwang@cug.edu.cn

J. Yu
ARC Centre of Excellence for Nanoscale BioPhotonics (CNBP)
School of Chemistry and Physics
The University of Adelaide
Adelaide, South Australia 5005, Australia
E-mail: Jingxian.Yu@adelaide.edu.au

H. Nara
Research Organization for Nano and Life Innovation
Waseda University
513 Waseda-tsurumaki-cho, Shinjuku-ku, Tokyo 162-0041, Japan

H. Nara, Y. Yamauchi
JST-ERATO Yamauchi Materials Space-Tectonics Project
4-1-8 Honcho, Kawaguchi, Saitama 332-0012, Japan

J. Na
International Center for Materials Nanoarchitectonics (MANA)
National Institute for Materials Science (NIMS)
1-1 Namiki, Tsukuba, Ibaraki 305-0044, Japan

J. Na, Y. Yamauchi
School of Chemical Engineering and Australian Institute for Bioengineering and Nanotechnology (AIBN)
The University of Queensland
Brisbane, Queensland 4072, Australia
E-mail: y.yamauchi@uq.edu.au

The ORCID identification number(s) for the author(s) of this article can be found under https://doi.org/10.1002/aenm.202002523.

DOI: 10.1002/aenm.202002523

electrode materials have the advantages of being lightweight and having high specific capacity, low environmental footprints, diverse molecular structures, and controllable design. Organic electrode materials are regarded as next-generation electrode materials with great application prospects.[8,19–22] Among the various organic materials, there are six types of materials that have been studied and determined to have application potential: conductive polymers,[23] organic sulfides,[24] organic radicals,[25] carbonyl compounds,[26] imine compounds, and azo compounds.[26–31]

In recent years, to continue to explore more organic materials that can be applied to rechargeable electrodes, the element N, which has an electronegativity close to that of O, has attracted substantial attention. Many articles have been reported on the application of organic compounds with nitrogen-containing groups (OCNs) as electrode materials. It can be seen that the electrochemical active sites containing the element N can play the role of electrochemical reaction centers and offer the following advantages. 1) OCNs can provide more Li storage sites per unit active site than other materials can. 2) OCNs have large insoluble frameworks to store Li^+ and simultaneously improve the inertness of dissolution. 3) OCNs can provide high electronic conductivity due to their high nitrogen content. 4) The heteroaromatic N atoms of OCNs can increase the redox potential. Moreover, the different mechanisms of metal ion insertion and extraction in OCNs have been gradually revealed.

However, the roles of N in these organic molecules are different. There are few reports summarizing and comparing electrochemical active organic compounds based on N sites. Therefore, to study this kind of molecule more deeply and systematically, it is necessary to summarize the application of these molecules in alkali metal rechargeable batteries with organic electrolytes and explore the corresponding laws for the application of OCNs.

Here, based on the clues obtained from atoms to molecules and from groups to molecules, for the N element, this paper reviews the current research status of OCNs as electrodes materials. The challenges faced by OCNs in alkali metal rechargeable batteries with organic electrolytes are reviewed, the improvement strategies determined by comparing the related scientific rules of nitrogen-containing groups and structures are proposed, and the direction of the research and development of OCNs in alkali metal rechargeable batteries with organic electrolytes are pointed out. In addition, the electrochemical contribution and kinetic behavior of the nitrogen atoms in active centers are also summarized.

2. Classification of OCNs

According to the second row in the periodic table, the electronegativity of N is between that of C and O. Combining the three elements of C, N, and O two by two (**Table 1**), the molecular structures with electrochemical activities can be listed. It is found that there are corresponding organic molecules containing each structure. Organic molecules containing C=C and C≡C have an extremely high capacity density when they are superlithiated.[27,32,33] The combination of oxygen and oxygen is O_2. C=O in organic carbonyl compounds is considered to be an electrochemical active structure with great application prospects and has been significantly studied.[34] The element N with an electronegativity close to that of O also has an electrochemical activity and exists in the electrochemical active centers of OCN molecules to undergo redox reactions. This is the subject of this article.

OCNs are defined as electrochemical active organic molecules containing the element N in their active centers. The process of the insertion and extraction of metal ions takes place in the active sites containing N in OCNs during charge and discharge. Some co-coordination of the N and O in C=O to metal ions is beyond the scope of this paper, because N is not in the electrochemical active center and plays an auxiliary role. In this work, we reviewed the OCNs that have been applied to alkaline metal ion batteries in recent years. According to the different active nitrogen-containing structural elements, based on carbon–nitrogen groups (C=N and C≡N), nitrogen–nitrogen groups (N=N) and nitrogen–oxygen groups (nitroxyl radicals and nitro groups) and covalent organic frameworks (COFs) in OCNs based on nitrogen-containing groups, OCNs are divided into four categories (**Figure 1**).

Table 1. Electrochemical active molecular structures composed of C, N, and O.

	C	N	O
C	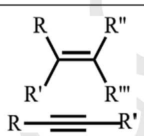	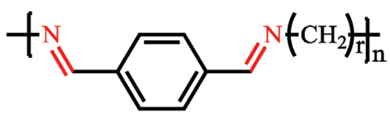	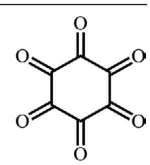
N	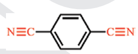	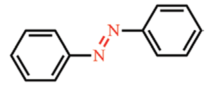	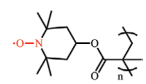
O	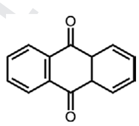	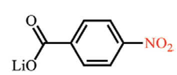	O_2

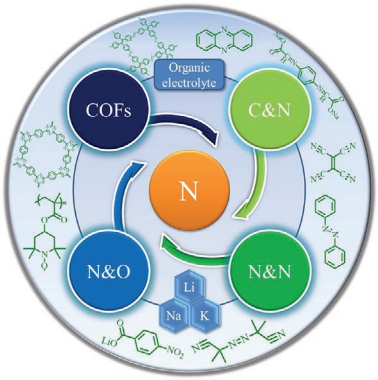

Figure 1. Electrochemical active OCNs.

3. Electrochemical Characteristics of OCNs

3.1. OCNs Based on Carbon–Nitrogen Groups

3.1.1. OCNs Based on C=N

There are many organic molecules containing the electrochemical active group C=N. According to the position of C=N in the organic molecular skeleton, these organic molecules can be divided into Schiff bases and other organic molecules with C=N as the active center. The electrochemical activity of C=N in the chain or heteroaromatic structure is quite different.

Schiff Bases: Schiff bases (**Figure 2**) containing Schiff functional groups ($R_1HC{=}NR_2$) are usually obtained by the condensation reaction of carbonyl-containing aldehydes, ketones, and amines.[35] Generally, the C=N groups exist in the chain structure of the Schiff base compounds.

Not all C=N groups in Schiff bases have obvious electrochemical activities since the electrochemical activity is related to the planarity and conjugation of the molecules. The reported redox centers include two Schiff functional groups attached to the benzene ring −N=CH−Ar−HC=N− (Ar indicates a benzene ring). These cyclic coplanar units follow the Hückel rule of aromaticity and contain $(4n + 2)$ π electrons ($n = 1, 2...$).[13,36] Similarly, the carboxylate group and C=N in the end group −OOC−Ar−C=N− that has 10 π-conjugated electrons are electrochemical active. DFT calculations indicate that the abovementioned two repeating units provide storage locations for Na^+. One active Hückel group is capable of inserting two sodium ions, corresponding to two single-electron reactions (**Figure 3**a).[37] The first electron forms a radical anion in equilibrium between the azo group and carbo radical (involving dimerization), and the second electron yields the dianion.[36]

The isomerization phenomenon will weaken the planarity of Schiff base molecules. The electrochemical activities of −CH=N−Ar−N=CH- and $-^{-}$OOC−Ar−N=C− are lower than those of their isomers −N=CH−Ar−CH=N− and end groups $-^{-}$OOC−Ar−C=N−. The reason for this may be that when the benzene ring is coplanar with the rest of the molecules in this unit, the strong electron interaction between the unpaired electrons of N and the π electron cloud of the adjacent aromatic ring leads to the loss of the planarity.[13,35,36] The compound with isomer (No. 1) shows the smallest reversible capacity due to its low activity. No. 2 and No. 3 with end groups $-^{-}$OOC−Ar−C=N− have a higher reversible capacity than No. 4 and No. 5 with isomeric units and the same length (Figure 3b). The electrochemical activity of No. 4 and No. 5 originates from the active center −N=CH−Ar−CH=N− in the middle of the molecules where Na^+ inserts. −Ar−CH=N−, with higher planarity than −Ar−N=CH−, is more conducive to Na^+ insertion.[36]

Aromatic rings can enhance the planarity of Schiff base molecules. The benzene rings between the Hückel active groups provide high planarity, and the π−π interaction between benzene rings further improves the crystallinity, making it easier to maintain planarity in aromatic-linked Schiff bases.[35] For example, the compounds without benzene rings in the middle (No. 6 and No. 7) have a lower capacity than No. 2.

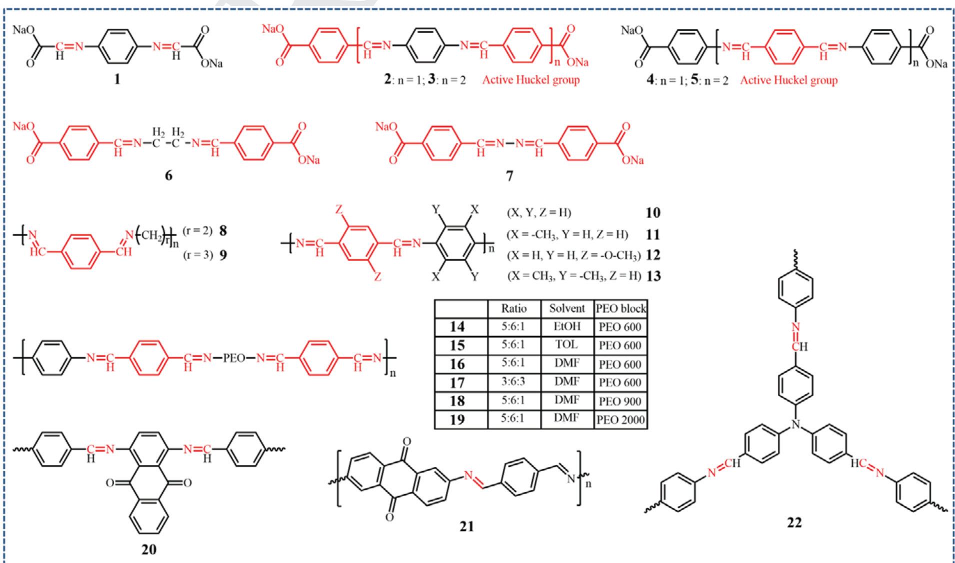

Figure 2. Schiff bases of OCNs (No. 1–22).

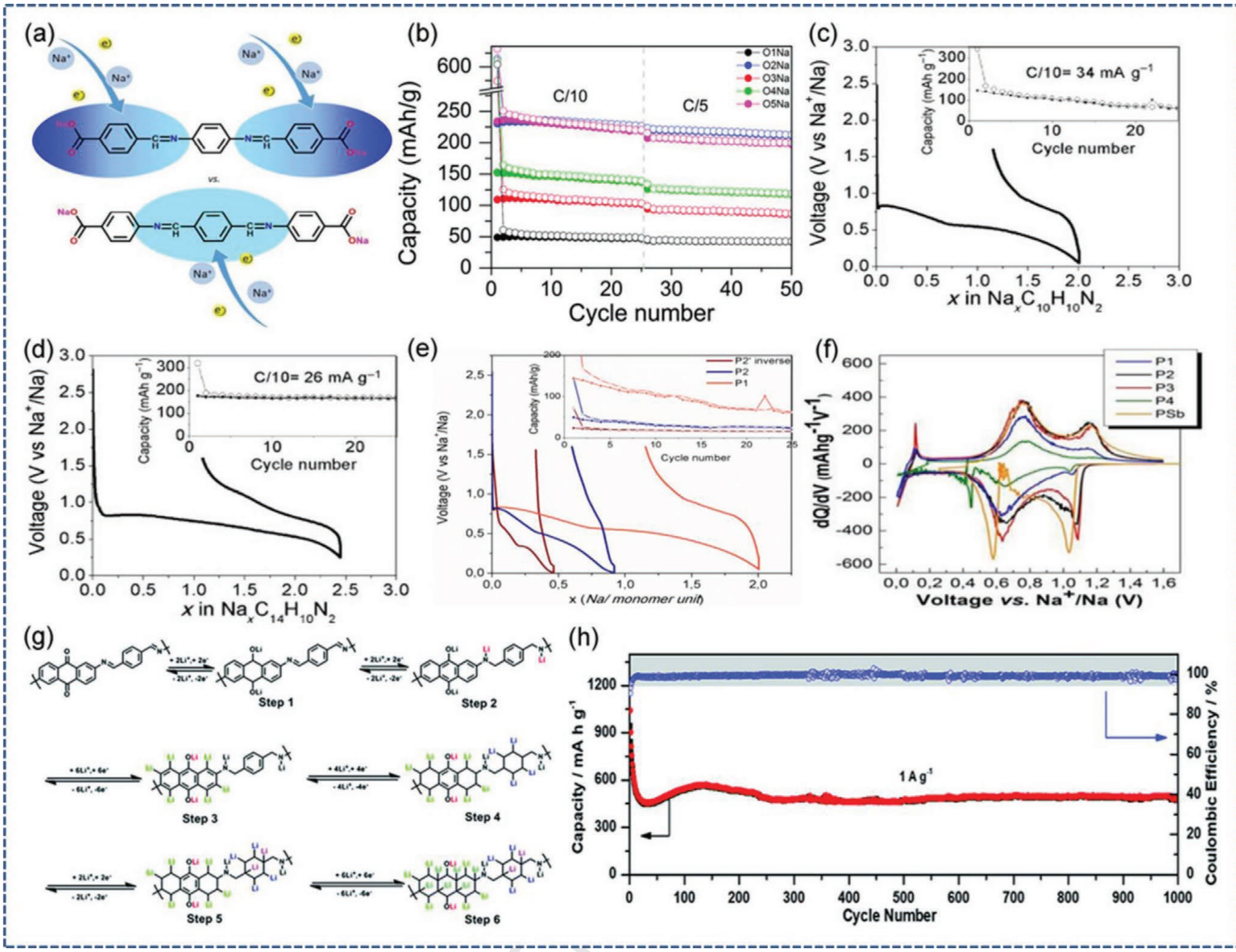

Figure 3. a) Electrochemical active centers in the Schiff bases. b) Cycle performance for oligomers No. 1–5 (O1Na-O5Na)[36] (Reproduced with permission.[36] Copyright 2015, Royal Society of Chemistry). Galvanostatic voltage profiles versus the number of sodium ions and electrons inserted, and the capacity versus cycle number during the first reduction and oxidation cycle of c) No. 8 and d) No. 10. e) Voltage versus specific capacity for the first galvanostatic reduction and oxidation cycle of No. 8 (P1), No. 9 (P2), and inverse No. 9 (inverse P2)[35] (Reproduced with permission.[35] Copyright 2014, Wiley-VCH). f) $\delta Q/\delta V$ versus voltage curves corresponding to the second cycle of No. 14–17 and No. 10 (P1–P4 and PSb)[38] (Reproduced with permission.[38] Copyright 2018, Wiley-VCH). g) Predicted mechanism of a reversible six-step Li^+ insertion/extraction reaction with No. 21. h) Cycle performance at a current density of 1 A g^{-1} of No. 21[39] (Reproduced with permission.[39] Copyright 2019, Royal Society of Chemistry).

Similarly, the stable capacity of No. 10 is ≈180 mAh g^{-1}, which remains almost unchanged after 6 cycles, while No. 8 has a capacity loss of 60% (Figure 3c,d).

Aliphatic hydrocarbon groups reduce the planarity of Schiff base molecules. According to their position, aliphatic hydrocarbon groups are divided into the aliphatic hydrocarbon structure between the Hückel active groups and the aliphatic hydrocarbon substituent on the benzene ring in the Hückel active groups. The very long aliphatic chains between the Hückel active groups will reduce π stacking inside the molecule so that the planarity weakens, and the capacity fades rapidly.[35] For example, No. 9 with more middle methylene groups has a greater capacity decay than No. 8 (Figure 3e). The insertion of the inactive PEO unit in the middle block (Nos. 14–19) will reduce the planarity, resulting in low capacity, but the extended π spacing is beneficial to the insertion of sodium, increasing the reduction voltage (Figure 3f).[38] The aliphatic hydrocarbon substituents on the benzene ring in the Hückel active groups will also reduce the planarity and crystallinity of the molecule, resulting in capacity reduction.[35] The difference between the capacity of No. 10 and the capacity of No. 11 and No. 12 with two substituents stems from the slight change in the capacity caused by the increase in mass, while No. 13 with four substituent groups undergoes obvious capacity decay due to its low planarity.

To further increase the capacity of the Schiff bases, some Schiff base polymers that combine other active groups or extend the conjugated structure were prepared. A polymeric Schiff base with anthraquinone as a linker that has two active units of C=N and C=O (No. 20, Figure 2) was prepared and showed a considerable performance without sacrificing capacity.[40] A highly conjugated poly(imine-anthraquinone) structure

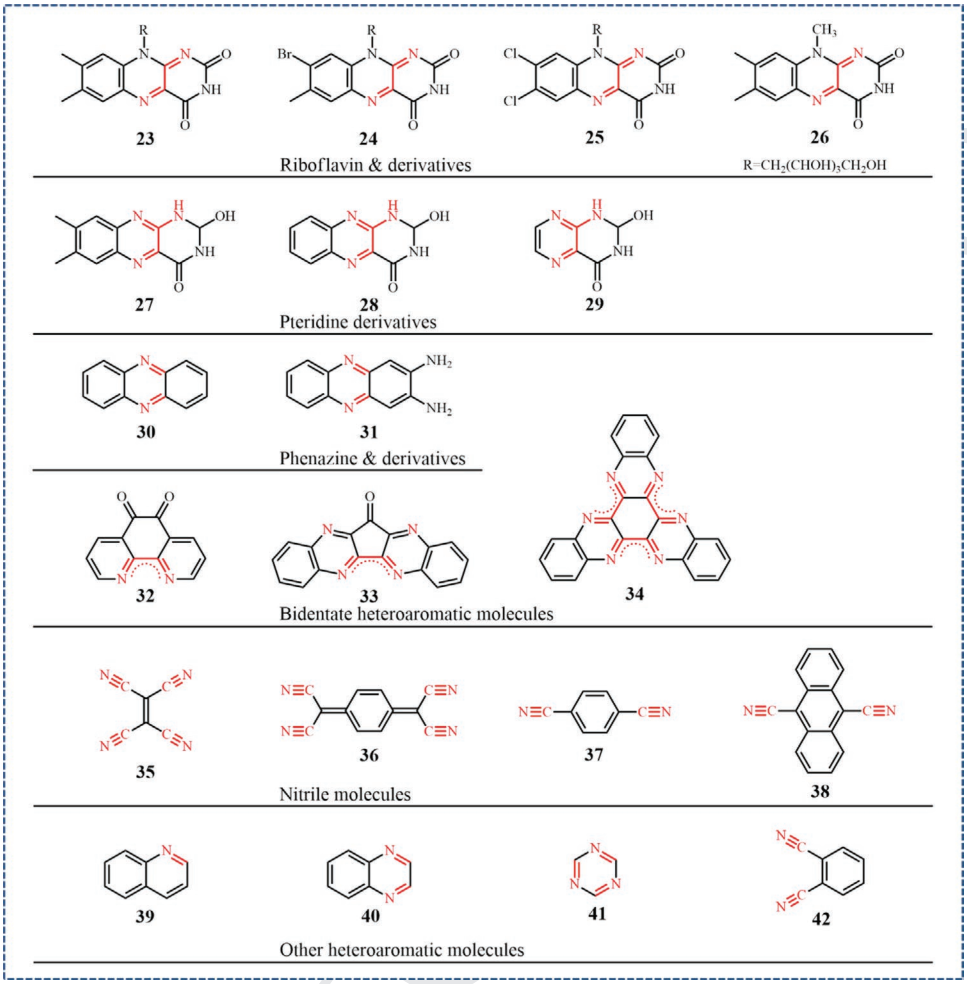

Figure 4. The first row is riboflavin and its derivatives, the second row is pteridine derivatives, the third row is phenazine and its derivatives, the fourth row is nitrogen-containing heteroaromatic molecules, the fifth row is nitrile molecules, and the sixth row is other OCNs based on C=N in heteroaromatic molecules (No. 23–42).

(No. 21, Figure 2) was prepared using a similar strategy, and the process of its superlithiation was studied (Figure 3g). The resulting poly(imine-anthraquinone) structure has a very high specific capacity and good cycle stability (Figure 3h).[39] A hyperbranched Schiff base polymer with a large conjugated structure was synthesized (No. 22, Figure 2). Due to the high degree of π-conjugation, this hyperbranched Schiff base polymer exhibits excellent electrochemical reversibility and lithium storage stability.[41]

OCNs based on C=N in Heteroaromatic Molecules: In addition to Schiff bases, there are riboflavin and its analogs, pteridine derivatives, phenazine, and its derivatives and other heteroaromatic molecules. This type of C=N exists in heteroaromatic active organic molecules.

Inspired by the proton-coupled electron transfer reaction of flavin molecules in nature, bionic electrode materials were applied in the batteries.[42] Each molecular unit of riboflavin (also called vitamin B_2) and its analogs (No. 23–26, **Figure 4**) is capable of inserting two Li^+. This reaction mainly occurs on the N atoms of isoximidine and tetraoximidine (**Figure 5**a), and the O atom in the carbonyl group also assists the reaction.[43] The redox potentials of No. 24 and No. 25 obtained by the substitution of Br or Cl atoms were increased by 0.09 and 0.14 V, respectively. No. 26 is fixed on the highly conductive single-walled carbon nanotubes (SWCNTs) through π–π interactions, thereby greatly improving the rate and cycle performance.[44] Reversible tautomerization occurs when Li^+ inserts in the pteridine derivatives.[45] In NIBs, the initial capacities provided by lumichrome (LC, No. 27), alloxazine (ALX, No. 28), and lumazine (LMZ, No. 29) are 138, 168, and 70 mAh g^{-1}, respectively. After compounding with CNTs, the capacities achieved by LC, ALX, and LMZ increased to 255, 225, and 220 mAh g^{-1}, respectively.

Phenazine (No. 30) and its aminated derivatives (DAP, No. 31) were applied in LIBs.[46] Due to the presence of the amino group, DAP's dissolution in an organic electrolyte is suppressed, thus achieving good cycle reversibility and high rate performance. Because the C=N bond has a rich electron density, lithium atoms tend to adsorb to the N atom in the C=N bond. During the charge and discharge process of the DAP electrode, only the conjugated C=N bond participates in the redox reaction in the lithium insertion and extraction

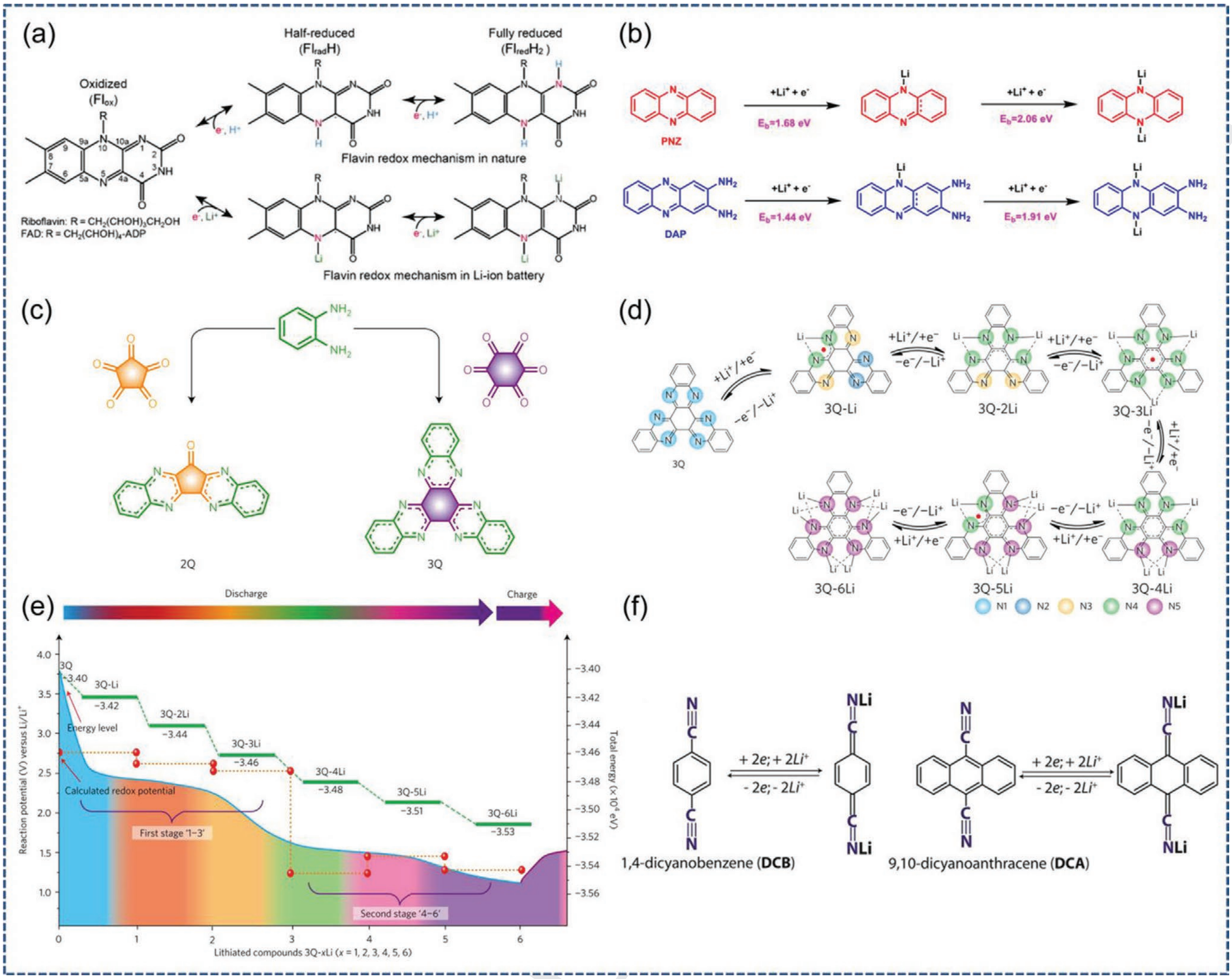

Figure 5. a) Different redox states of flavin molecules with indications of redox-active parts upon electron uptake[43] (Reproduced with permission.[43] Copyright 2013, Wiley-VCH). b) Lithiation and binding energies of No. 30 and No. 31 with lithium atoms[46] (Reproduced with permission.[46] Copyright 2017, Royal Society of Chemistry). c) Synthetic scheme of No. 33 and No. 34. d) The predicted lithiated structures of 3Q during the discharging process. e) The discharge curve is marked by the blue line, and the shaded and colored areas indicate the evolution of various lithiated 3Q structures[47] (Reproduced with permission.[47] Copyright 2017, Springer Nature). f) The proposed electrochemical mechanism for No. 37 and No. 38 in Li-ion batteries[48] (Reproduced with permission.[48] Copyright 2017, Elsevier).

process (Figure 5b) and can achieve reversible fracture and generation.

Heteroaromatic molecules designed by molecular engineering strategies also have good electrochemical activity. 4,5-Diaza-9,10-phenanthrenequinone (No. 32, Figure 4) was used as the cathode active material of LIBs.[49] No. 32 has large coordination energy, and the chelation of N—N0 has a stable effect on Lithium ion. The quinoxaline derivatives diquinoxalinylene (2Q, No. 33, Figure 4) and triquinoxalinylene (3Q, No. 34, Figure 4) were applied as the cathodes of LIBs and were prepared through the condensation of cyclic carbonyl molecules with o-phenylenediamine (Figure 5c).[47] The N atoms in 3Q are capable of forming bidentate sites for lithium ions to gradually insert 6 lithium ions (Figure 5d), in which 5 N resonance states form. The 3Q DFT simulation is consistent with the discharge curve, forming two platforms in the range of 2.6–2.15 V and 1.68–1.38 V (Figure 5e). 2Q and 3Q have good intrinsic conductivity because of their low energy gaps, and the extended π conjugation makes the charge exchange between molecules and lithium ions easier, resulting in an excellent rate performance.[47]

3.1.2. OCNs Based on C≡N

In OCNs based on carbon–nitrogen groups, in addition to molecules based on C=N, the molecules based on C≡N are also applied to LIBs and NIBs. In 1990, a Na/β''-alumina/TCNE half-cell operating at 230 °C was reported.[50] According to FTIR spectra, C≡N and C=C are electrochemical active sites.[13] After that, DFT calculations showed that 4 Li^+/Na^+, 5 Li^+/Na^+, and 2.5/2 Li^+/Na^+ can be inserted in tetracyanoethylene (TCNE, No. 35), TCNE adsorbed on graphene and the covalent crystal TCNE, respectively.[51,52] The surface science experiments were used to study Li^+/Na^+ insertion in tetracyanoquinodimethane (TCNQ, No. 36) and its effect on the electronic structure, showing that TCNQ is capable of inserting two Li^+/Na^+.[53,54] TCNQ was applied as the cathode of a quasi-solid electrolyte battery.[55] The discharge capacity reached 215.8 mAh g^{-1} for the first cycle at 0.2 C and maintained ≈170 mAh g^{-1} after 100 cycles. 1,4-Dicyanobenzene (No. 37) and 9,10-dicyanoanthracene (DCA, No. 38) based on C≡N were applied as the anode materials in LIBs.[48] One C≡N is capable of inserting one Li^+ to form −C=N−Li (Figure 5f). Due to the large aromatic π-conjugated skeleton, DCA exhibits good electrochemical stability and a low lowest unoccupied molecular orbital (LUMO) level, which is conducive to withdrawing electrons and achieving high electronic conductivity. Moreover, the long DCA framework leads to a strong C≡N induction effect and electron-withdrawing ability, showing a high redox potential.[56] Recently, studies have shown that the C≡N groups at the first and second positions of the aromatic ring are co-coordinated with Li^+.[57] These studies may indicate that the charging and discharging mechanisms of OCNs based on C≡N will be different due to the relative positions of C≡N. Therefore, specific molecules need to be discussed in detail.

3.1.3. Summaries

This section reviews OCNs based on carbon–nitrogen groups (C=N, C≡N) reported in recent years. C=N can extend the molecular skeleton and increase the inertness of dissolution while inserting metal ions as dual/multifunctional sites. Although the electrochemical activity of C=N, which is composed of C and N with a lower electronegativity than that of O, is relatively low, there are still two strategies for enhancing the electrochemical activity of C=N. 1) In the chain structure, the electrochemical activity of C=N can be enhanced by satisfying the active structure or rule (the Hückel rule). 2) In a heteroaromatic molecule, the electrochemical activity of C=N can be enhanced through the extension of the conjugated structure. Since C≡N is an end group, the structural adjustability of organic molecules based on C≡N is lower than that based on C=N. At present, there are few nitrile molecules applied in rechargeable batteries that are still worthy of further research. However, the OCNs based on carbon–nitrogen groups still face the problem of a low theoretical capacity density ($C_{\mathrm{theoretical}}$), and the energy density needs to be further improved.

From the current research, the development of OCNs based on carbon–nitrogen groups offers the following directions. 1) Combining OCNs with other active groups through polymerization. 2) Studying more molecular configurations based on OCNs (such as No. 39–42 and its isomers or derivatives). 3) Designing new OCNs with molecular engineering strategies. 4) Studying organic macromolecules based on the active structures in Figure 4, such as polymers. 5) Further improving the electronic conductivity to reduce the content of conductive additives, for example, increasing the N content and doping iodine.[58]

3.2. OCNs Based on Nitrogen–Nitrogen Groups

3.2.1. Azo Compounds

Azo compounds are formed by connecting an azo group −N=N− with two hydrocarbon groups. The general formula of azo compounds is R−N=N−R′. Azo compounds are a new type of electrochemical active organic material and can be divided into aromatic azo compounds and aliphatic azo compounds (**Figure 6**).

Aromatic Azo Compounds: Aromatic azo compounds have a π-conjugated structure with an azo group that connects two benzene rings to extend the conjugated structure. Since the electron-withdrawing effect of N and the unshared p-electron pair cause delocalization of the benzene ring by the conjugation effect, the electron cloud density of the benzene ring increased, and the insertion of Li^+ was promoted.[59] Taking No. 46 as an example (**Figure 7**a), the XRD patterns and Raman spectra (Figure 7b,c) show that when discharging from 3 to 1 V, N=N can be reduced to Li−N−N−Li as two Li^+ are inserted, and Li−N−N−Li returns to N=N after charging from 1 to 3 V as two Li^+ are extracted.

In the same battery systems, the addition of carboxylate groups to electrochemical active organic molecules can effectively increase the polarity of the organic molecules, thereby reducing the solubility in an organic electrolyte and inhibiting the shuttle effect.[61,62] The electrochemical performances of aromatic azo compounds in LIBs and NIBs were studied according to this strategy.[28–30] The dissolution of aromatic azo compounds in organic electrolytes is inhibited because of the addition of carboxylate groups, and the inhibitory action and the improvement in the electrochemical performance can be superimposed. In LIBs, the electrochemical performances of azobenzene (AZOB, No. 43), 4-(phenylazo)benzoic acid lithium salt (PBALS, No. 44), methyl red sodium salt (No. 45), and azobenzene-4,4′-dicarboxylic acid lithium salt (ADALS, No. 46) show an increasing trend. The initial capacity of ADALS at 0.5 C is 190 mAh g^{-1}, and the reversible capacity maintained after 100 cycles is 175 mAh g^{-1}, with a fairly small decrease after 2000 cycles (Figure 7d,e). The rules are the same in NIBs: azobenzene-4,4′-dicarboxylic acid sodium salt (ADASS, No. 48) has better cycle stability and higher reversible capacity than AZOB and 4-(phenylazo)benzoic acid sodium salt (PBASS, No. 47) (Figure 7f,g).

Azo compounds with similar molecular skeletons have different charge and discharge potentials in different batteries. The charge/discharge potential of AZOB in LIBs is higher than that in NIBs. PBALS (in LIBs) and PBASS (in NIBs) with similar molecular skeletons are the same as AZOB. The charge/discharge potential of aromatic azo compounds with two carboxylate groups follows the order of ADALS > Azobenzene-4,4′-dicarboxylic acid potassium salts (ADAPTS, No. 49, Figure 6) > ADASS. The reason for this trend is that K/K^+ has a redox potential of −2.93 V, which is close to the redox potential of Li/Li^+ (−3.04 V vs. standard hydrogen electrode) and is 200 mV lower than the redox potential of Na/Na^+ (−2.71 V), resulting in KIBs having a higher voltage and energy than NIBs in principle.[14,63,64]

The N=N group plays a central role in the electrochemical performance of aromatic azo compounds. 1) N=N not only provides electrochemical activity for aromatic azo compounds but also manifests a larger amount of $Li^+/Na^+/K^+$ inserted per

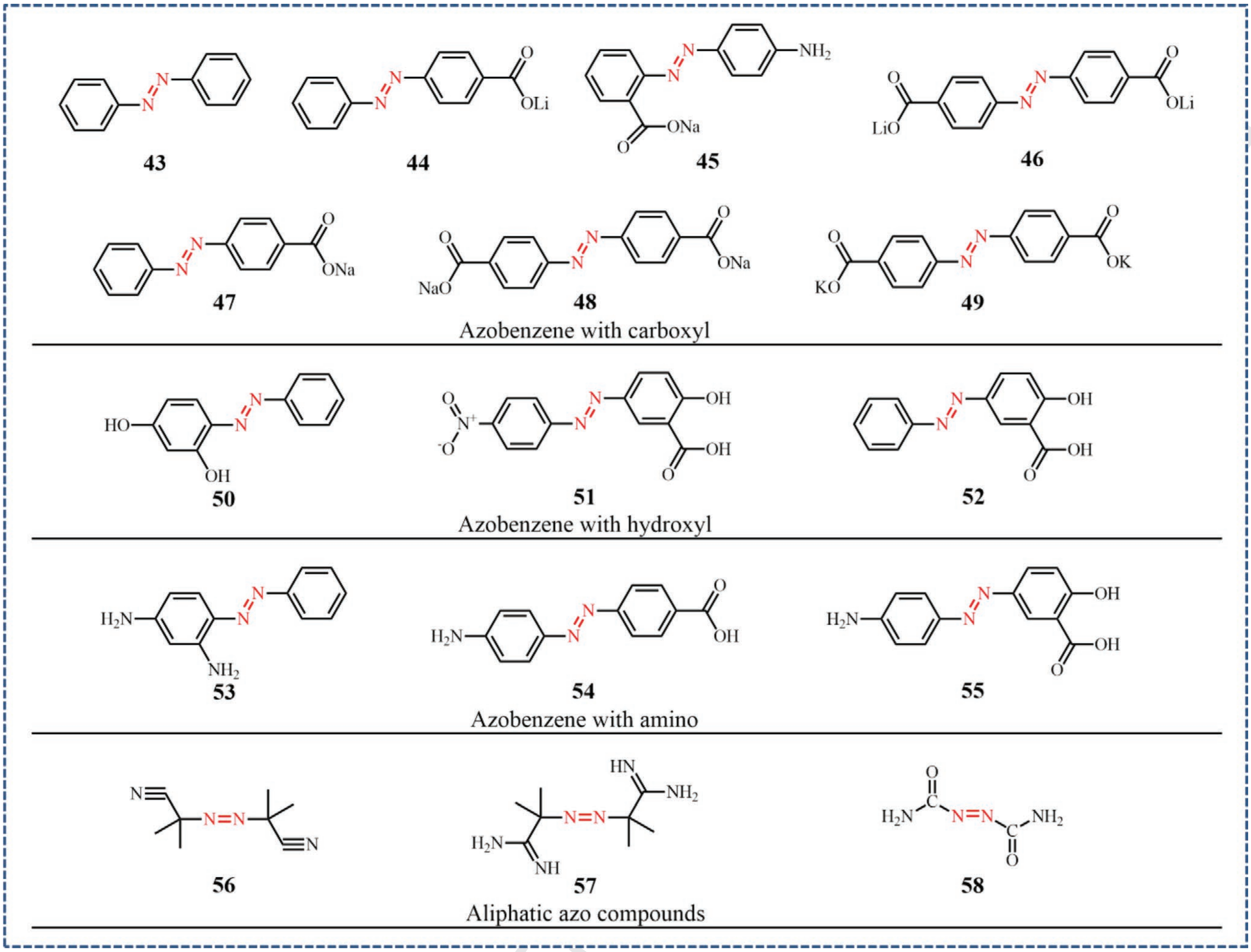

Figure 6. Aromatic azo compounds (No. 43–58).

active unit.[28–31] 2) Compared to C=O, whose dipole moment formed because the electronegativity of C is less than that of O, resulting in the electrons of C being biased toward O,[60] N=N is more stable because the two N atoms have the same electronegativity. Whether in LIBs, NIBs, or KIBs, the discharge platform of azo compounds is almost always in the range of 1.0–2.0 V. In addition, in an all-solid electrolyte battery, the charge transfer between PBALS and a Li_3PS_4 (LPS) SSE hardly affects the activity of N=N, and the specific capacity is maintained (Figure 7h,i).[60] 3) The two N atoms in N=N are easily conjugated with the adjacent aromatic ring, making the azo bond conductive. From the DFT calculation, the lithium carboxylate group also improves the intrinsic electronic conductivity of aromatic azo compounds (Figure 7j).[28] The collective effect of N=N conductivity and carboxylate groups confers ADALS, ADASS, and ADAPTS with good rate performance in LIBs, NIBs, and KIBs, respectively. The reasons why aromatic azo compounds have a fast charge/discharge capability and relatively long cycle life are the extension of the π-conjugated structure and the strong attraction of azo groups to metal ions.[28]

Aliphatic Azo Compounds: 2,20-Azobis(2-methylpropionitrile) (AIBN, No. 56), 2,20-azobis(2-methylpropionamidine) dihydrochloride (AIBA, No. 57) and azodicarbonamide (CONH, No. 58), which contain N=N as the active center and C=N and C=O, were applied in rechargeable batteries.[65] These three aliphatic azo compounds have high theoretical capacities, and AIBN (326.4 mAh g^{-1}), AIBA (593.4 mAh g^{-1}), and CONH (923.5 mAh g^{-1}) do not contain a benzene ring. The discharge capacity of AIBN in KIBs is much higher than that in LIBs and NIBs. There are two N=N and C=N active sites in AIBA, in which the performance is moderate during the 500 cycles in the LIBs. Because the structure of AIBA is more stable after the transformation, the Li insertion space increases, and the capacity steadily increases. When CONH is applied as an anode in NIBs, N=N and C=O are both active sites for Na^+ extraction. The good capacity retention of CONH is attributed to its stable crystal structure, and CONH minimally interferes with Na^+ due to its large radius.

3.2.2. Summaries

Here, OCNs based on nitrogen–nitrogen groups are summarized, and these OCNs are mainly small molecule azo compounds. Azo compounds are a new type of electrochemical

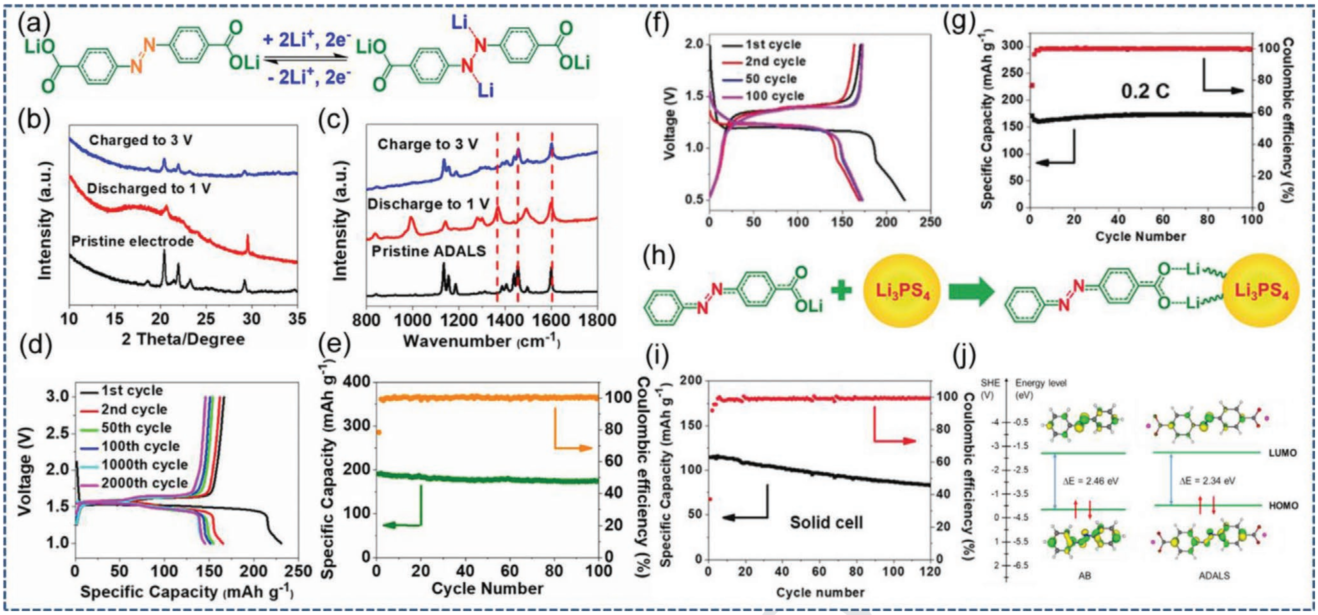

Figure 7. a) Reaction mechanism of ADALS. b) XRD patterns of ADALS electrodes before and after five cycles. c) Raman spectra of ADALS electrodes before and after five cycles. d) The galvanostatic charge/discharge profiles of ADALS at 2 C. e) Delithiation capacity and Coulombic efficiency versus cycle number at a current density of 0.5 C[28] (Reproduced with permission.[28] Copyright 2018, PNAS). f) The galvanostatic charge/discharge profiles of ADASS at 0.2 C. g) Desodiation capacity and Coulombic efficiency versus cycle number at a current density of 0.2 C[29] (Reproduced with permission.[29] Copyright 2018, Wiley-VCH). h) Interaction between PBALS and LPS. i) Delithiation capacity and Coulombic efficiency of PBALS during charge/discharge cycles performed at 20 mA g^{-1} in SSE[60] (Reproduced with permission.[60] Copyright 2018, Wiley-VCH). j) DFT calculation results obtained for the relative energies and optimized structures of AZOB and ADALS[28] (Reproduced with permission.[28] Copyright 2018, PNAS).

active material. Azo groups have the advantage of providing many Li storage sites per unit active site. High solubility and poor long cycle stability are the main problems of small azo molecules. The strategy of enhancing the polarity can effectively inhibit the solubility of small azo molecules and improve the electrochemical performance. The application of other performance improvement strategies in azo compounds necessitates further study. Small azo molecules that can be used as organic electrodes in alkali metal rechargeable batteries should have two characteristics. 1) They should have groups that can increase the inertness of dissolution (−COOH, −OH, $-NH_2$, etc.) and can even be further made into salts (including Li salt, Na salt, and K salt). 2) The azo group should be directly connected to the benzene ring. According to numerous reports, the presence of benzene rings in organic molecules plays an active role overall. When the active site is directly connected to the benzene ring, the large π-conjugated system is conducive to intermolecular charge transfer due to the extended conjugated structure.[22] The large aromatic π-conjugated skeleton makes organic molecules have a low LUMO, which is conducive to electron withdrawal, and high electronic conductivity.[48] The addition of a benzene ring can improve the planarity and crystallinity of the molecule, making the insertion of metal ions easier.[13,36] Based on this, some promising azobenzene small molecules (No. 50–55) can be speculated from the structure to explore the roles of $-NH_2$ and −OH and their influences on the performances of aromatic azo compounds under coaction with −COOH. The other two directions are researching long-chain aromatic azo compounds and compounding them with insoluble conductive substrates.

3.3. OCNs Based on Nitrogen–Oxygen Groups

OCNs based on nitrogen–oxygen groups mainly include nitroxyl radicals and other molecules containing nitrogen–oxygen active groups (**Figure 8**).

3.3.1. Nitroxyl Radicals

Nitroxyl radicals contain unpaired electrons that are moderately delocalized at the center of N−O, resulting in the partial π bonds of N−O bonds.[66] In 2002, the organic radicals were used as electrode materials in LIBs for the first time.[25] In alkali metal ion batteries, such OCNs are composed of polymers with pendant stable organic radicals, most of which are reported to be nitroxyl radicals based on nitro groups.[27,67] Nitroxyl radicals are relatively stable in the redox process, with little structural change.[68] Therefore, nitroxyl radicals usually exhibit rapid reaction kinetics and low voltage polarization.[27]

Nitroxyl Radicals Based on (2,2,6,6-Tetramethyl-1-Piperidinyl)Oxyl: Nitroxyl radical polymers based on the redox center (2,2,6,6-tetramethyl-1-piperidinyl)oxyl (TEMPO) are the most attractive of the nitroxyl radicals.[68] The electron transfer process of such radicals includes two steps: the first step is the heterogeneous electron transfer of the current collector to the radical component, and the second step is the homogeneous charge transfer between the radical parts.[67–69] The redox reaction is a one by one two-electron reaction process, corresponding to the redox reactions between the TEMPO radical and ammonium anion (n-type doped state) in the range of 2.5–3.0 V and between the

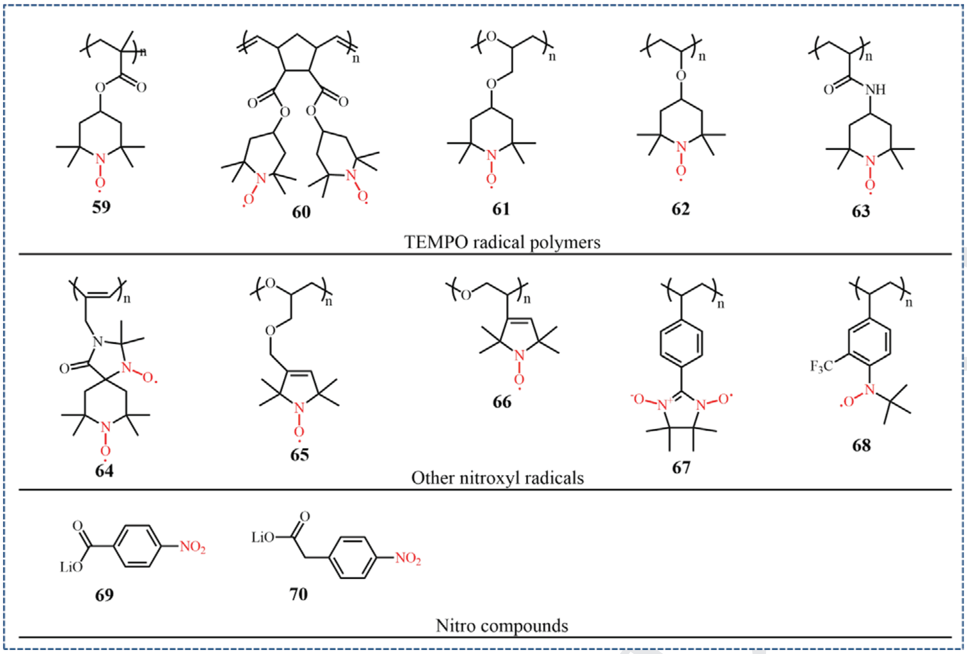

Figure 8. TEMPO radical polymers, other nitroxyl radicals, and nitro compounds (No. 59–70).

TEMPO radical and oxoammonium cation (p-type doped state) near 3.6 V (**Figure 9**a).[70,71] The oxidation-reduction potentials of different TEMPO radicals change slightly.

One of the most frequently studied nitroxyl radicals is poly(2,2,6,6-tetramethylpiperidinyloxy methacrylate) (PTMA, No. 59), which undergoes minor structural changes and electron rearrangements during the redox process[25,27,73–75] To improve the electronic conductivity while suppressing the dissolution of PTMA in the organic electrolyte, a positive electrode compounded with graphene was prepared, which has an excellent rate performance and a long cycle life[70] The PTMA/CNT-array electrodes were used to reduce the charge transfer impedance between PTMA and a current collector[76] Similarly, an active polymer was encapsulated in carbon nanotubes to form a high-polymer-content PTMA-impregnated-CNT electrode used as a cathode for NIBs[69] The hollow structure of CNTs can wrap PTMA and inhibit dissolution. At the same time, many CNTs form a stable network structure to provide an effective conductive path (Figure 9b,c). The filling of PTMA in CNTs was confirmed by TEM and other characterization methods (Figure 9d), and the content of PTMA in the electrode was analyzed by TGA. The batteries based on the PTMA-impregnated-CNT electrode have two plateaus at ≈2.51 V and ≈3.51 V and high specific capacities close to $C_{theoretical}$ (Figure 9e). Furthermore, the charge transfer impedance is also significantly lower than that of the conventional composite (Figure 9f), as the charge transfer impedance of the PTMA-impregnated-CNT electrode remains almost unchanged at 217 mAh g^{-1} after 100 cycles at 0.5 C. In addition, electrochemical performance tests on PTMA with different degrees of polymerization (DPs) show that a higher degree of polymerization is conducive to the improvement in the performance of free radical polymers (Figure 9g), because PTMA with a low degree of polymerization is more soluble in the electrolyte than PTMA with a high DP[72]

The second electrochemical active nitroxyl radical based on TEMPO is poly(TEMPO-substituted norbornene) (No. 60), which has two TEMPO structures per molecule unit[67,77–79] No. 60 was applied to all radical polymer batteries[80] After that, applied poly(TEMPO-substituted norbornene) was applied as a cathode in NIBs[81] The maximum initial discharge capacity of the battery at a current density of 50 mA g^{-1} is 75 mAh g^{-1}, and the discharge capacity retention rate after 50 cycles is 64.5%.

Other nitroxyl radicals based on the TEMPO structure have also been studied. The cathode of cross-linked poly(2,2,6,6-tetramethylpiperidinyl-*N*-oxyl glycidyl ether) (PTGE, No. 61) was polymerized with the organic ion conductor PEO combined with CNTs, resulting in a discharge capacity of 93 mAh g^{-1}, which is 90% of the $C_{theoretical}$[82] The pristine poly(4-vinyloxy-2,2,6,6-tetramethyl-piperidine-*N*-oxyl) (PTVE, No. 62) material exhibited a low lithium activity due to its poor electronic conductivity. Benefiting from the electronic conductivity and structural stability provided by the 3D network structure of graphene, the initial discharge capacity of a PTVE/graphene nanocomposite at 1 C can reach 96% of the $C_{theoretical}$, which is higher than that of the control group without graphene. This nanocomposite can still maintain a capacity of 152 mAh g^{-1} after 20 000 cycles performed at a high rate of 100 C[71] In addition, No. 63, which has a skeleton similar to that of PTMA, has been applied to batteries but has not been applied to alkaline metal rechargeable batteries in organic electrolytes[83]

Other Nitroxyl Radicals: The application of other nitroxyl radicals to increase the capacity in alkali metal rechargeable batteries with organic electrolytes has also been reported[67] Spiro-bisnitroxide (No. 64) contains another nitroxyl radical added to the repeating unit to increase its specific capacity[84] However, the lithium battery test shows that only radicals based on six-membered rings undergo a reversible redox reaction. The 2,2,5,5-tetramethylpyrrolidin-*N*-oxyl radical based on

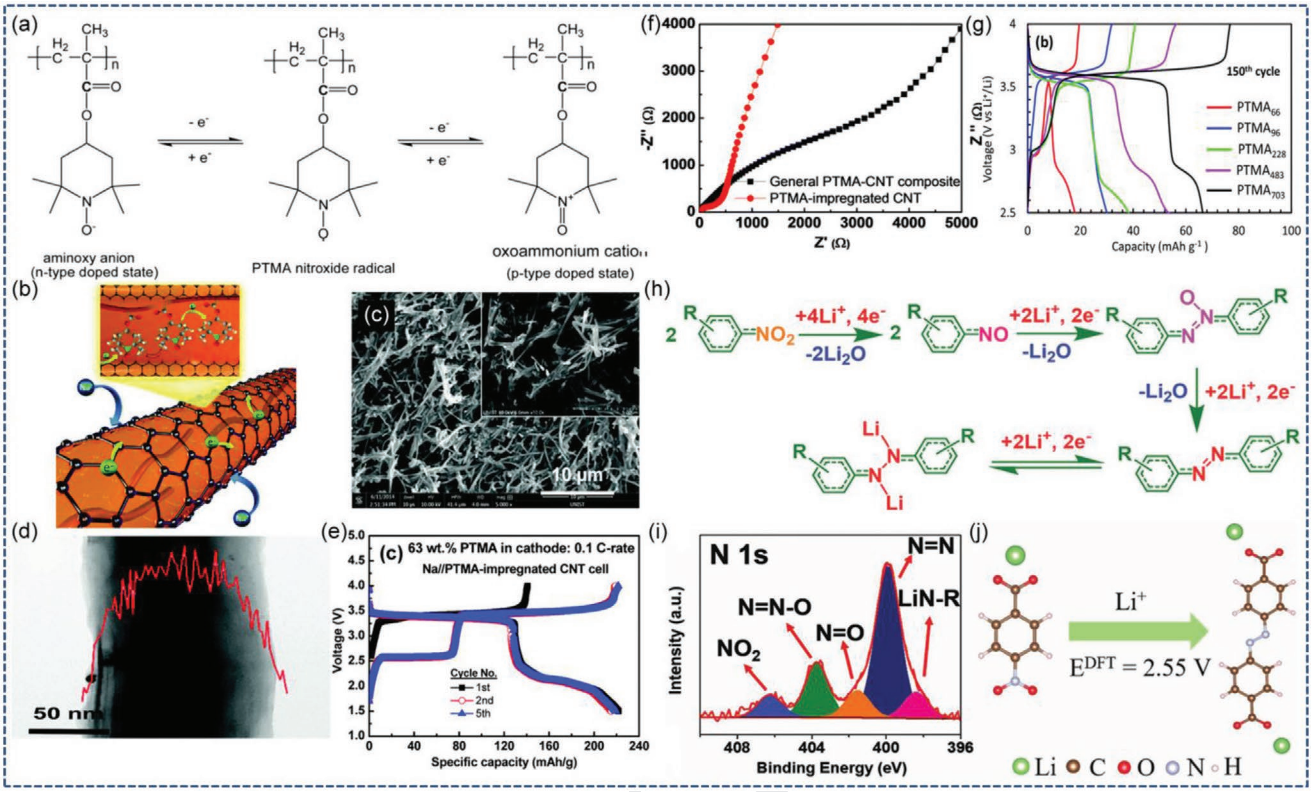

Figure 9. a) Redox couples of PTMA[70] (Reproduced with permission.[70] Copyright 2012, Royal Society of Chemistry). b) Schematic illustration of the PTMA-impregnated CNT structure. c) SEM images of PTMA-impregnated CNT electrodes. d) TEM images of PTMA-impregnated CNTs and EDX line scanning of the C atom along the cross-section. e) The galvanostatic charge/discharge profiles at the first, second and fifth cycles of the PTMA-impregnated CNT sodium battery at room temperature. f) Impedance spectra of PTMA-impregnated CNT electrodes[69] (Reproduced with permission.[69] Copyright 2016, Royal Society of Chemistry). g) The charge/discharge specific capacity of PTMA with different DPs at the 150th cycle[72] (Reproduced with permission.[72] Copyright 2017, Royal Society of Chemistry). h) Reaction mechanism of nitro-based organic materials. i) N 1s XPS spectra of NBALS electrodes after 1 cycle. j) The illustration and calculated equilibrium potentials (EDFT vs. Li/Li^+) for the reduction of NBALS to an azo compound[30] (Reproduced with permission.[30] Copyright 2018, Wiley-VCH).

a five-membered ring and with a mass less than the TEMPO radical based on a six-membered ring has a higher theoretical ratio capacity than the TEMPO radical. The reduction potential of No. 65 is ≈3.66 V, which is slightly higher than that of PTMA. The discharge capacity at 10 C is ≈80 mAh g^{-1}, and the capacity retention rate after 100 cycles is more than 90%[85] T The reduction potential of No. 66 is ≈3.7 V, the discharge capacity at 10 C is ≈90 mAh g^{-1}, and the capacity retention after 1000 cycles is more than 80%[66] However, the experimental discharge capacity of the aforementioned free radicals is lower than 100 mAh g^{-1}, resulting in the advantage of good cycle stability. In addition, the redox reactions of nitrostyrene polymers (No. 67 and No. 68) have been studied[86,87] Due to the strengthening of conjugation, the nitroxyl radicals are stabilized by the benzene ring, but these nitroxyl radicals have not been applied to alkali metal rechargeable batteries with organic electrolytes.

3.3.2. Other OCNs Based on Nitrogen–Oxygen Groups

It has been reported that nitro groups are also electrochemical active centers[30] By comparing the differences between the electrochemical performances of 4-nitrobenzoic acid lithium salt (NBALS, No. 69), 4-nitrophenylacetic acid lithium salt (No. 70) and BALS, it was indicated that the carboxyl group was not involved in the redox reaction, and electrochemical activity originates from the nitro group. Moreover, the nitrobenzene compounds were irreversibly transformed into amorphous azo compounds during the first discharge cycle (Figure 9h), which was proven by XPS and XRD characterization methods and electrochemical tests (Figure 9i). The reduction potential calculated by DFT in this process is very close to the experimental value (Figure 9j). Similar to nitro groups, nitroso groups may also have some electrochemical activity, but their stability during charging and discharging and changes to other substances have not yet been determined.

3.3.3. Summaries

OCNs based on nitrogen–oxygen groups are reviewed in this section. Among these OCNs, nitroxyl radicals are potential electrode materials for alkali metal rechargeable batteries with organic electrolytes. Nitroxyl radicals with the TEMPO structure are still the main object of organic radical research, and

PTMA is the mainstream. The nitroxyl group provides electrochemical activity but also its high activity also makes the nitroxyl radical have fast reaction kinetics so that the assembled battery has a higher redox voltage. Moreover, the combination of nitroxyl radicals and carbon materials can greatly increase the specific capacity and effectively improve the rate performance and long cycle stability. This suggests that the application of nitroxyl radicals in ORBs has great research prospects. However, due to the complicated preparation process and molecular structure, nitroxyl radicals contain few active sites and have a low specific capacity. At the same time, the common problems of the high solubility and low conductivity of organic molecules still restrict the application of nitroxyl radicals in alkali metal rechargeable batteries with organic electrolytes. In addition, the reported nitro redox reaction is not reversible, and its application potential needs to be further tapped. In response to the abovementioned conditions, other OCNs based on nitrogen–oxygen groups need to be explored, and more in-depth studies of the researched substances are also required. For example, the reaction mechanism of other nitroxyl radicals, the improvement in the conductivity through the composite conductive substrate, and the influence of the molecular weight of nitroxyl radicals on the capacity, etc., should be studied.

3.4. COFs in OCNs

Compared with conventional small organic molecules and polymers, COFs are more promising candidates for electrode materials in rechargeable batteries due to their high specific surface area, porous structure, and low electrode volume change[27,88–90] The specific capacity of COFs comes from the insertion of alkali metal ions in the active site and the capacitance capacity caused by the porous structure. On the one hand, a large molecular weight inhibits dissolution and improves cycle stability. On the other hand, the porous skeleton shortens the path of ion diffusion[91] Among them, COFs based on nitrogen-containing sites have gradually attracted attention (**Figure 10**). COFs based on nitrogen-containing sites can be divided into three categories according to the different active nitrogen-containing groups.

3.4.1. COFs Based on Carbon–Nitrogen Groups

The C=N group in the chain of COFs is formed by the Schiff base reaction and exists in the form of a skeleton connecting COFs. The controlled growth of few-layered 2D COFs (No. 71) on CNTs was realized (**Figure 11**a), which not only improves the conductivity of the electrode material but also eliminates

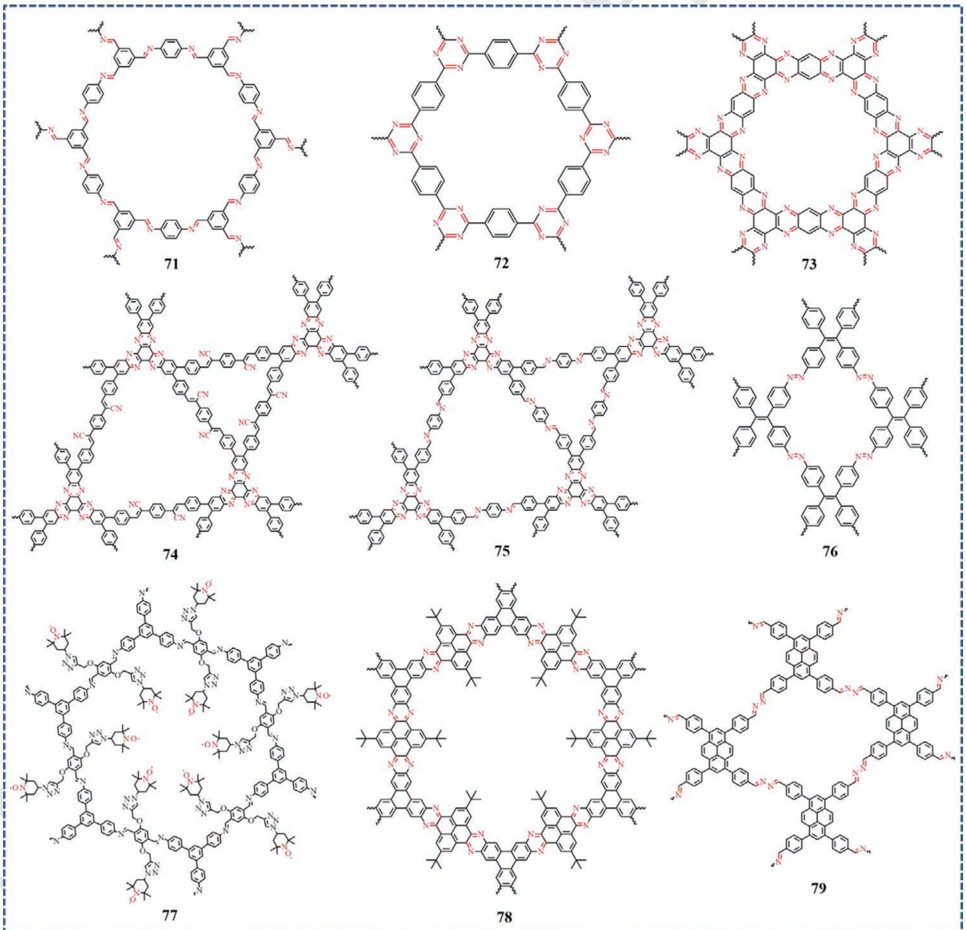

Figure 10. COFs in OCNs (No. 71–79).

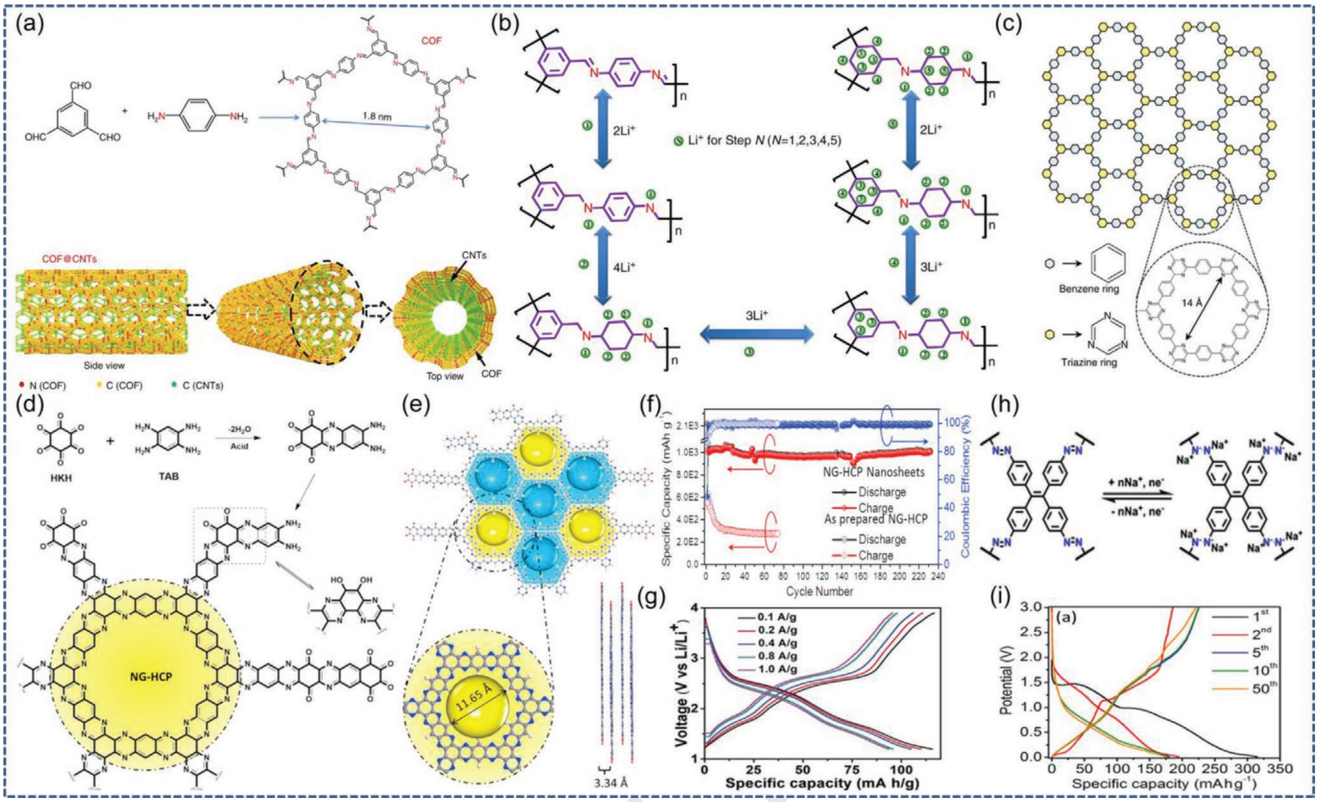

Figure 11. a) Growth of a COF on CNTs. b) Five-step lithium insertion and extraction reaction with a COF[92] (Reproduced with permission.[92] Copyright 2018, Springer Nature). c) The 2D structure of the BPOE is composed of triazine rings and benzene rings[92] (Reproduced with permission.[92] Copyright 2013, Springer Nature). d) Dehydration–condensation in an NMP solution and schematic representation of the pristine NG-HCP structure. e) Molecular configuration of a single layer NG-HCP with 11.65 Å micropores and a packing distance of 3.34 Å. f) Cycling performance of NG-HCP nanosheets and a pristine NG-HCP anode hybrid with CNTs at a current density of 0.1 A g^{-1}[93] (Reproduced with permission.[93] Copyright 2017, Elsevier). g) The galvanostatic charge/discharge profiles of 2D CCP-HATN@CNT at different current densities[94] (Reproduced with permission.[94] Copyright 2019, Wiley-VCH). h) Synthesis of ALP-8 and its redox mechanism with sodium ions. i) The galvanostatic charge/discharge profiles of ALP-8 battery at 0.3 C[95] (Reproduced with permission.[95] Copyright 2019, American Chemical Society).

the insufficient utilization of the redox center caused by the close packing[92] Excluding the capacity contribution of CNTs, the capacity of COF@CNTs reaches 1032 mAh g^{-1} (100 mA g^{-1}, 500 cycles), which is much higher than the specific capacity of COFs directly used as electrode materials. The lithium-storage mechanism for COF in the COF@CNTs anode has also been revealed (Figure 11b). In fact, some hyperbranched Schiff base polymers, such as No. 22, can also be considered as such COFs.

The C=N group contained in the heteroaromatic molecules in COFs is mainly derived from the trimerization of nitrile groups and the synthesis of the phenazine structure[96] The bipolar function of amorphous covalent triazine-based frameworks (ACTF-1) in LIBs was studied[97] A bipolar porous organic electrode (BPOE, No. 72) composed of benzene and a triazine ring was synthesized and used as a cathode in NIBs (Figure 11c). The p-doping process on the surface of BPOE occurs in the range of 4.2–2.8 V, and n-doping and Na^+ insertion on BPOE occur in the range of 2.8–1.3 V[98] BPOE's special porous structure is conducive to electrolyte infiltration, while its high molecular weight inhibits dissolution, thereby showing high capacity retention of 80% after 7000 cycles. Due to the bipolar function of BPOE, it has a very high power density and a long cycle life when applied to all organic energy storage strategies[99]

Free-standing nitrogen-rich graphene-like HCP (NG-HCP, No. 73, Figure 11d,e) and nanosheets with far better performance than the original NG-HCP material produced through nanoengineering were reported[93] After 230 cycles, at a current density of 0.1 A g^{-1}, the reversible capacity of the NG-HCP nanosheets remained at a high value of ≈1015 mAh g^{-1} (Figure 11f), and the NG-HCP nanosheets showed an excellent rate performance. On the one hand, this excellent rate performance is obtained because the high specific surface area and large reaction contact area of NG-HCP after nanoengineering promote the charge transfer reaction. On the other hand, the addition of heteroatoms (such as nitrogen atoms) to the conjugated COF structure provides the enhanced electrochemical reactivity of NG-HCP, resulting in the excellent battery performance of the electrode material.

It is reported that a 2D SP^2-carbon chain conjugated polymer (2D CCP) framework 2D CCP-HATN (No. 74) based on nitrogen-rich hexanaphthalene (HATN) and the corresponding imine cross-linked COF analog 2D C=N HATN (No. 75) have been applied to LIBs[94] 2D CCP-HATN has a better redox performance than 2D C=N HATN. After in situ growth on carbon nanotubes (CNTs) to improve the conductivity of 2D CCP-HATN, the prepared 2D CCP-HATN@CNT core-shell hybrid material exhibited a high capacity (116 mAh g^{-1}) and high redox-active unit (HATN) utilization. 2D CCP-HATN@CNT also presented symmetrical charge/discharge curves with the high reversibility of the electrochemical redox process (Figure 11g).

3.4.2. COFs Based on Nitrogen–Nitrogen Groups

COFs containing N=N are synthesized, and N=N plays the dual roles of connecting the molecular backbone and providing the active site. The azo-linked polymers (ALP-8, No. 76) are used as the cathode in NIBs (Figure 11h)[95] The sodiation of ALP-8 is a mixing process that includes Na^+ insertion into the polymer and surface pseudocapacitance Na^+ storage. The process of sodium insertion is the same as that of the insertion of small molecules. During discharge, two Na^+ ions insert in N=N to form Na—N—N—Na, and N=N recovers as Na^+ is extracted during charging. Due to the complex electronic properties and redox reactions in the amorphous framework, the charge/discharge curves gradually become sloping (Figure 11i). After 150 cycles, the specific discharge capacity of 170 mAh g^{-1} is maintained, and the capacity retention exceeds 90%. The pseudocapacitance stems from the porous structure of ALP-8. N=N mainly exists in the chain, so the structural diversity of the corresponding COFs is lower than that of COFs containing C=N; in addition, the number of N=N groups in COFs is also low.

3.4.3. COFs Based on Nitrogen–Oxygen Groups

Few-layer 2D nanosheets of TEMPO-ECOF (No. 77) were prepared by ball milling and post-synthesis modification[100] Due to the strong π—π interaction, the pristine COFs are often aggregated together, which inevitably leads to the insufficient utilization of redox-active sites, thereby reducing their capacity and rate performance. For comparison, the capacity of the stripped TEMPO-ECOF is 53% higher than that of its pristine material at 20 mA g^{-1}. TEMPO-ECOF shows two discharge platforms at 3.6 and 2.7 V, and the corresponding redox reaction is consistent with the principle of the TEMPO radical. TEMPO-ECOF prepared by stripping has the characteristics of atomic control and high crystallization, and its capacity and potential can be fine-tuned, providing a platform for better understanding the diffusion mechanism of the active center and the electrochemical process[23] and providing new strategies for improving the electrochemical performance of COFs in batteries.

3.4.4. Summaries

Electrochemical active COFs based on nitrogen-containing sites are summarized here. Based on the advantages of COFs, a variety of nitrogen-containing sites, including C=N in the chain, C=N in heteroaromatic molecules, C≡N, N=N, and TEMPO radicals, improve the application potential. However, there is no denying that low conductivity is still an obstacle for the application of COFs in rechargeable batteries[96] Currently, combining COFs with carbon materials is the best way to improve the conductivity of COFs,[101] and increasing the number of nitrogen atoms in the repeating unit is also a strategy. The mechanism of the reaction needs to be further explained. Recent studies have shown that there are radicals in the charge and discharge process of DAAQ-COF[102] In addition, it can be observed that the number of active sites in each repeating unit of COFs in OCNs is relatively small. Therefore, working with other active groups to increase the average number of active sites in each repeating unit is a strategy to increase the specific capacity. Such groups, such as anthraquinone structure and polyimide, can be added before the synthesis of COFs or modified after synthesis[88,101–104] Some COFs containing C=N (No. 78 and No. 79) were successfully synthesized, and COFs in nanoporous films were prepared. However, these materials have not been used in batteries[105–108] Therefore, the application of COFs in rechargeable batteries has great prospects, but further research is still needed.

3.5. Metal-Organic Frameworks with OCNs

Metal-organic frameworks (MOFs) are a class of developing energy storage materials, which are usually composed of variable valence metal ions (such as transition metal ions) and/or redox-active ligands[109] Due to high porosity, multifunctionality and diverse structures, MOFs can be used not only as additives but also as electrode active materials in rechargeable batteries. Although MOFs with OCNs as organic linkers in rechargeable batteries have not been reported, their application prospects are still worth discussing.

MOFs can store lithium (sodium) ions by intercalation/deintercalation or conversion reaction mechanisms. The introduction of organic ligands with redox activity is a strategy to improve the specific capacity of MOFs, which can participate in the redox reaction together with metal elements. Awaga and colleagues reported an MOF, Cu(2,7-AQDC) (2,7-H2AQDC = 2,7-anthraquinonedicarboxylic acid), with independent redox-active sites on $Cu_2(Ac)_4$ paddlewheels and anthraquinone groups in the ligand, which resulted in a high initial capacity of 147 mAh g^{-1}[110] This proves that electrochemical active organic molecules can be used as electrode materials in MOFs. It is speculated that OCNs have the same application potential. This also provides a new strategy to expand the application of OCNs as electrode materials.

4. Analysis and Simulation Calculation

Routine electrochemical tests can determine the rich electrochemical parameters of OCNs. Due to the structural characteristics of OCNs, their molecular structures can be designed and assembled according to their electrochemical reaction process. In this work, the simulation calculation can do more with less.

4.1. Analysis and DFT Calculation of OCNs

4.1.1. Analysis of OCNs

The distribution range of the average discharge potential of electrochemical active organic compounds based on different

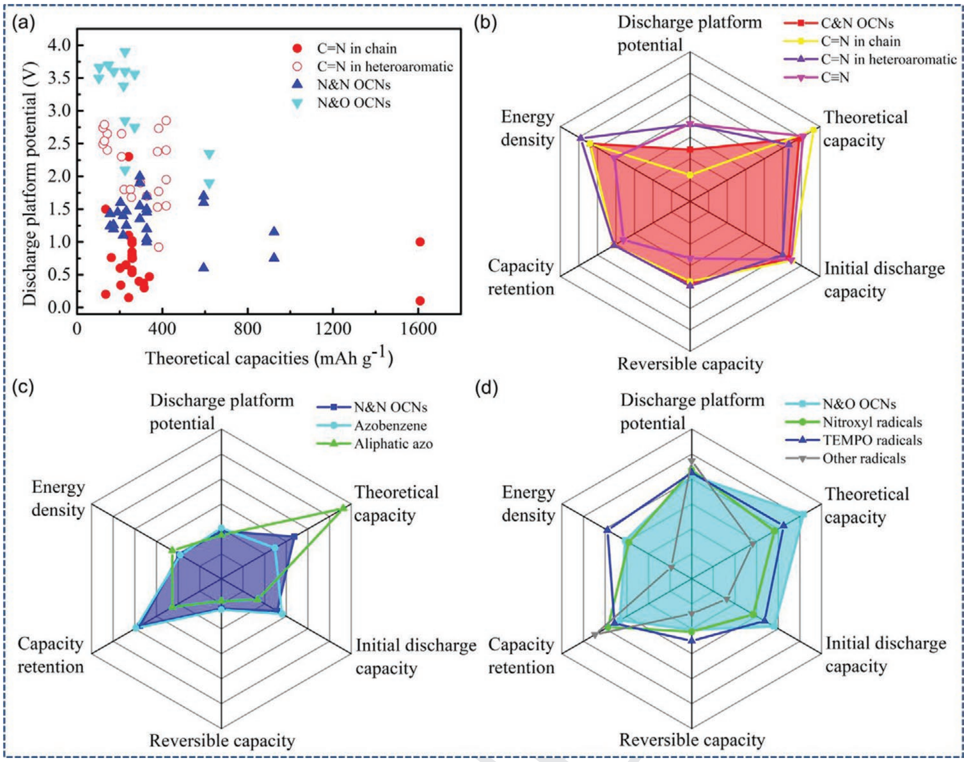

Figure 12. Overview of the fundamental properties of various types of OCNs. a) The discharge platform potentials of OCNs. OCNs based on b) carbon–nitrogen groups, c) nitrogen–nitrogen groups, and d) nitrogen–oxygen groups. The data are from **Table 2**.

nitrogen-containing groups is different (**Figure 12**a), which is caused by the different electronegativity of the elements that make up the active site. For OCNs based on carbon–nitrogen groups, the average discharge potential of the compounds with C=N in their chains is mainly distributed below 1.5 V (red solid points), while the average discharge potential of the compounds with C=N in their heteroaromatic groups is mainly distributed between 1.5–3.0 V (red hollow dots). For OCNs based on nitrogen–nitrogen groups, the average discharge potential of azo compounds is mostly between 1.0–2.0 V (blue triangles), and the individual reduction potential of aliphatic azo compounds is below 1.0 V. For OCNs based on nitrogen–oxygen groups, due to the existence of bipolar compounds, the reduction potential is mainly distributed between 2.0–4.0 V (light blue triangles).

The differences between the performances of the electrochemical active substances based on the same nitrogen-containing group stem from the differences in their molecular structures. For OCNs based on carbon–nitrogen groups (Figure 12b), the reason why the discharge platform of C=N in heteroaromatic molecules is higher than that of C=N in chains is that the electrochemical activity of the former is higher than that of the latter, and the heteroaromatic N can also increase the reduction potential due to the extension of the conjugated structure. Although C≡N is an electron-withdrawing group that can increase the working potential, nitrile molecules have a strong solubility and rapid capacity decay, which leads to low reversible capacity and energy density. For OCNs based on nitrogen–nitrogen groups (Figure 12c), the aliphatic azo compounds have no benzene ring, so their $C_{\text{theoretical}}$ is higher than the capacity of aromatic azo compounds. However, the conjugation of aliphatic azo compounds is weak, resulting in a strong solubility and low capacity retention, reversible capacity, and initial capacity. By contrast, azobenzene compounds have higher capacity retention. For OCNs based on nitrogen–oxygen groups (Figure 12d), the dissolution problem decreases the reversible capacity and capacity retention of nitroxyl radicals. However, the OCNs based on nitrogen–oxygen groups also show high reduction potential because of the high activity of radicals. The electrochemical performance of other radicals is weaker than that of TEMPO radicals. This may be due to the presence of conjugates, such as olefin in an electron-rich state, and so it is not easy to combine additional electrons, making the n-type doping process difficult. Overall, the TEMPO radicals are preferable to other nitroxyl radicals.

4.1.2. DFT calculation of OCNs

Here, to further understand the differences between the electrochemical activities of various OCNs, the LUMO, the highest occupied molecular orbital (HOMO) and energy gap of some typical published and unpublished compounds were calculated by DFT (**Figure 13**a). The low LUMO levels of various OCNs indicate their good electron affinity and high reduction potential. Both OCNs based on carbon–nitrogen groups and nitrogen–nitrogen groups have low energy gaps, indicating their good intrinsic conductivity. In contrast, the nitroxyl radicals in the OCNs based on nitrogen–oxygen groups have large energy gaps, indicating poor conductivity, and two pairs of LUMOs and HOMOs correspond to two doping processes.

Table 2. Summary of the electrochemical properties of OCNs. A) Number. B) Molecular weight (M_w) of monomer. C) Theoretical specific capacities ($C_{theoretical}$ = nF/3.6 M_w, where n is the transferred electron number, and F is the Faraday constant. For Schiff compounds and COFs, $C_{theoretical}$ is determined according to the literature or calculated by the mechanism. For pteridine derivatives and azo compounds, n is the number of conjugated N atoms. For radical compounds, *n* is the number of radicals.). D) Electrode composition (*X* indicates the active material, and the ratio is the mass ratio.). E) Voltages of discharge/charge platform or average voltages (*V*). F) First discharge and charge capacities (mAh g^{-1}). G) Discharge capacities (mAh g^{-1})/current/cycles. H) Discharge capacities (mAh g^{-1}) with high rate/current. I) Electrodes versus the reference electrode. J) Notes and references.

A	B	C	D	E	F	G	H	I	J
No. 1	264	161	X:Carbon Super C-65 (Imerys): Ketjen Black (KB) = 80:15:5	0.76/1.18	50/	50/0.1 C/25		Anode versus Na/Na^+	Binder free[36]
No. 2	416	258	X:Carbon Super C-65 (Imerys): KB = 80:15:5	0.85, 0.75, 0.53/1.01, 0.80, 0.62	268/250	225/0.1 C/25	80/2 C	Anode versus Na/Na^+	[36]
No. 3	623	258	X:Carbon Super C-65 (Imerys): KB = 80:15:5	1.02, 0.80, 0.57/1.15, 0.99, 0.65	260/248	220/0.1 C/25	80/2 C	Anode versus Na/Na^+	[36]
No. 4	416	258	X:Carbon Super C-65 (Imerys): KB = 80:15:5	0.99, 0.31/1.14, 0.87	120/125	100/0.1 C/25		Anode versus Na/Na^+	[36]
No. 5	623	258	X:Carbon Super C-65 (Imerys): KB = 80:15:5	0.98, 0.79/1.08, 0.81	150/160	125/0.1 C/25		Anode versus Na/Na^+	[36]
No. 6	368	291	X:Carbon Super C-65 (Imerys): KB = 80:15:5	0.4/0.7	213/220	100/_/10		Anode versus Na/Na^+	[36]
No. 7	340	315	X:Carbon Super C-65 (Imerys): KB = 80:15:5	0.3/0.7	/196			Anode versus Na/Na^+	[36]
No. 8	158	339	X:Carbon Super C-65 (Imerys) = 8:2	0.47/0.85	350/170	50/34 mA g^{-1}/25		Anode versus Na/Na^+	Binder free[35]
No. 9	172	312	X:Carbon Super C-65 (Imerys) = 8:2	0.37/0.79	140/60	20/_/25		Anode versus Na/Na^+	Binder free[35]
No. 10	206	260	X:Carbon Super C-65 (Imerys) = 8:2	0.75/0.95	310/180	180/26 mA g^{-1}/25		Anode versus Na/Na^+	Binder free[35]
No. 11	234	229	X:Carbon Super C-65 (Imerys) = 8:2	0.65/0.79				Anode versus Na/Na^+	Binder free[35]
No. 12	266	202	X:Carbon Super C-65 (Imerys) = 8:2	0.60/0.87				Anode versus Na/Na^+	Binder free[35]
No. 13	262	205	X:Carbon Super C-65 (Imerys) = 8:2	0.34/0.87				Anode versus Na/Na^+	Binder free[35]
No. 14			X:Carbon Super C-65 (Imerys) = 8:2	0.63, 1.09/	184/	116/19.7 mA g^{-1}/25		Anode versus Na/Na^+	Active materials double as binder[38]
No. 15			X:Carbon Super C-65 (Imerys) = 8:2	0.63, 1.09/	190/	158/19.7 mA g^{-1}/25		Anode versus Na/Na^+	Active materials double as binder[38]
No. 16			X:Carbon Super C-65 (Imerys) = 8:2	0.63, 1.09/	256/	178/19.7 mA g^{-1}/25	158/0.2 C/25	Anode versus Na/Na^+	Active materials double as binder[38]
			X:Carbon Super C-65 (Imerys) = 8:2	0.63, 1.09/		206/19.7 mA g^{-1}/25		Anode versus Na/Na^+	Laminate electrodes[38]
			X:Carbon Super C-65 (Imerys) = 9:1	0.63, 1.09/		100/19.7 mA g^{-1}/25		Anode versus Na/Na^+	Powder electrode[38]
			X:Carbon Super C-65 (Imerys) = 9:1	0.63, 1.09/		201/19.7 mA g^{-1}/25		Anode versus Na/Na^+	Laminate electrodes[38]
			X:Carbon Super C-65 (Imerys) = 1:1	0.63, 1.09/		316/19.7 mA g^{-1}/25		Anode versus Na/Na^+	[38]
			X:KB = 1:1	0.63, 1.09/		285/19.7 mA g^{-1}/25		Anode versus Na/Na^+	[38]
No. 17			X:Carbon Super C-65 (Imerys) = 8:2	0.63, 1.09/	266/	60/19.7 mA g^{-1}/25		Anode versus Na/Na^+	Active materials double as binder[38]
No. 18			X:Carbon Super C-65 (Imerys) = 8:2	0.63, 1.09/	230/	127/19.7 mA g^{-1}/25	106/0.2 C/25	Anode versus Na/Na^+	Active materials double as binder[38]

ADVANCED ENERGY MATERIALS
www.advenergymat.de

Table 2 Continued.

A	B	C	D	E	F	G	H	I	J
No. 19			X:Carbon Super C-65 (Imerys) = 8:2	0.63, 1.09/	229/	104/19.7 mA g^{-1}/25	81/0.2 C/25	Anode versus Na/Na^+	Active materials double as binder[38]
No. 20	443	242	X:super P (SP):polytetrafluoroethylene (PTFE) = 85:10:5	0.15, 1.1, 2.3/0.3, 1.0, 3.2	315/97	160/10 mA g^{-1}/100	40.3/80 mA g^{-1}	Anode versus Li/Li^+	[40]
No. 21	366	1609	X:KB:carboxymethylcellulose (CMC) = 7:2:1	1.0, 0.1/	1231/1130	1097/0.2 A g^{-1}/100	259/2.0 A g^{-1}	Anode versus Li/Li^+	[39]
No. 22	597	135	X:acetylene black (AB):PTFE = 5:4:1	0.2, 1.5/		127/1 C/500	60/16 C	Cathode versus Li/Li^+	[41]
No. 23	377	142	X:SP:PTFE = 5:3:2	2.65, 2.4/	105.88/			Cathode versus Li/Li^+	[43]
No. 24	441	122	X:SP:PTFE = 5:3:2	2.74, 2.49/				Cathode versus Li/Li^+	[43]
No. 25	417	129	X:SP:PTFE = 5:3:2	2.79, 2.54/				Cathode versus Li/Li^+	[43]
No. 26	256	209	X:SP:PTFE = 5:3:2	2.65, 2.3/	174.32/			Cathode versus Li/Li^+	[43]
No. 27	242	221	X:SP:PTFE = 4:4:2			169/20 mA g^{-1}/		Cathode versus Li/Li^+	[45]
	242	221	X:SP:PTFE = 4:4:2			181/20 mA g^{-1}/		Cathode versus Li/Li^+	60 °C[45]
	242	221	X:CNT = 43:57			215/220 mA g^{-1}	153/10 A g^{-1}	Cathode versus Li/Li^+	CNT hybrid[45]
	242	221	X:CNT = 43:57	1.8/2.0	222/	111/50 mA g^{-1}/20	138/10 mA g^{-1}	Cathode versus Na/Na^+	CNT hybrid[45]
No. 28	214	250	X:SP:PTFE = 4:4:2			181/20 mA g^{-1}/		Cathode versus Li/Li^+	[45]
	214	250	X:CNT = 41:59			236/250 mA g^{-1}	168/10 C	Cathode versus Li/Li^+	CNT hybrid[45]
	214	250	X:CNT = 41:59	1.8/2.0	255/	128/50 mA g^{-1}/20	168/10 mA g^{-1}	Cathode versus Na/Na^+	CNT hybrid[45]
No. 29	166	327	X:SP:PTFE = 4:4:2			154/		Cathode versus Li/Li^+	[45]
	166	327	X:SP:PTFE = 4:4:2			251/10 mA g^{-1}/		Cathode versus Li/Li^+	60 °C[45]
	166	327	X:CNT = 35:65	1.7/2.5	220/	110/50 mA g^{-1}/20	70/10 mA g^{-1}	Cathode versus Na/Na^+	CNT hybrid[45]
No. 30	180	297	X:SP:polyvinylidene fluoride (PVDF) = 6:3:1	1.9, 1.3/	205/	69.8/0.1 A g^{-1}/100		Cathode versus Li/Li^+	[46]
No. 31	210	255	X:SP:PVDF = 6:3:1	1.68/		220/0.1 A g^{-1}/100	93.3/2 A g^{-1}	Cathode versus Li/Li^+	[46]
No. 32	210	383	X:AB:PVDF = 1.5:4:1	2.73, 1.77, 0.92/					[49]
No. 33	284	377	X:graphene:PVDF = 3:6:1	2.7–2.5, 2.5–2.2, 2.2–1.8, 1.9–1.2/3.1–2.6, 2.6–2.2, 2.2–1.7, 1.7–1.4	395/	395/1 C/200	218/20 C	Cathode versus Li/Li^+	[47]
No. 34	384	418	X:graphene:PVDF = 3:6:1	2.11–2.95, 1.41–1.75/2.6–2.15, 1.68–1.38	372/	372/1 C/200	229/20 C	Cathode versus Li/Li^+	[47]
No. 36	204	263	X:KB:PTFE = 47.6:46.9:5.6	3.1, 2.5/	215.8/	170/.02 C/100		Cathode versus Li/Li^+	quasi-solid-state LIB[55]
No. 37	128	418	X:AB:PTFE = 5:4:1					Cathode versus Li/Li^+	[48]

Table 2 Continued.

A	B	C	D	E	F	G	H	I	J
No. 38	228	235	X:AB:PTFE = 5:4:1	1.79, 1.33/2.12, 1.67	330/184.8	96/_/30	134.0/50 $mA\ g^{-1}$	Cathode versus Li/Li^+	[48]
No. 43	182	294	X:carbon black (CB):PVDF = 6:3:1	1.9, 1.55/2.5, 1.8	103/	65/0.5 C/20		Cathode versus Li/Li^+	[28]
	182	294	X:CB:PVDF = 6:3:1	2.0, 1.35/	929/	15/		Cathode versus Na/Na^+	[29]
No. 44	232	231	X:CB:sodium alginate = 6:3:1	1.47, 1.25/1.30, 1.55, 2.0	220/	178/0.5 C/100	85/20 C	Cathode versus Li/Li^+	[30]
No. 45	263	204	X:CB:sodium alginate = 6:3:1	1.6/1.6	110/	110/0.5 C/30		Cathode versus Li/Li^+	[28]
No. 46	282	190	X:CB:sodium alginate = 6:3:1	1.45/1.55, 1.65	190/	175/0.5 C/100	105/20 C	Cathode versus Li/Li^+	[28]
No. 47	248	216	X:CB:sodium alginate = 6:3:1	1.4, 1.1/1.4, 1.1	162/	65/0.5 C/50		Cathode versus Na/Na^+	[29]
No. 48	314	171	X:CB:sodium alginate = 6:3:1	1.26, 1.2/1.43, 1.37	170/	170/0.2 C/100	71/40 C	Cathode versus Na/Na^+	[29]
No. 49	346	155	X:CB:sodium alginate = 6:3:1	1.43, 1.24/1.5	134/	109/0.1 C/100	66/10 C	Anode versus K/K^+	Room temperature[31]
	346	155	X:CB:sodium alginate = 6:3:1	1.43, 1.24/1.5			77/2 C/1000	Anode versus K/K^+	50 °C[31]
	346	155	X:CB:sodium alginate = 6:3:1	1.43, 1.24/1.5			98/4 C/90	Anode versus K/K^+	60 °C[31]
No. 56	164	326	X:SP:PVDF = 8:1:1	1.7, 1.2/	100/		30/50 $mA\ g^{-1}$	Anode versus Li/Li^+	[65]
	164	326	X:SP:PVDF = 8:1:1	1.5, 1.0/			70/50 $mA\ g^{-1}$	Anode versus Na/Na^+	[65]
	164	326	X:SP:PVDF = 8:1:1	1.45, 1.05/	200/	80/10 $mA\ g^{-1}$/100	80/50 $mA\ g^{-1}$	Anode versus K/K^+	[65]
No. 57	198	593	X:SP:PVDF = 8:1:1	1.7, 1.6, 0.6/			50/50 $mA\ g^{-1}$	Anode versus Li/Li^+	[65]
No. 58	116	924	X:SP:PVDF = 1:1:1	1.15, 0.75/			224.5/5 $mA\ g^{-1}$	Anode versus Na/Na^+	[65]
No. 59	231	225	X:CB:PVDF = 1:8:1	3.6, 2.8–3.0/3.6, 2.8–3.0	166/120	76/1 C/100		Cathode versus Li/Li^+	[70]
	231	225	X:graphene:CB:PVDF = 1:6:2:1	3.5–3.7, 2.5–3.2/3.5–3.7, 2.5–3.2	222/250	169/1 C/100	80/200 C	Cathode versus Li/Li^+	PTMA/graphene composite[70]
	231	225	X:CNT:PVDF = 3:6:1	3.6/3.6		80/1 C/100	63/100 C	Cathode versus Li/Li^+	PTMA/CNT-array electrode[76]
	231	225	X:CB:PVDF = 63:30:7	2.2/3.0	142/61		10/5 C	Cathode versus Na/Na^+	General PTMA–CNT composite[69]
	231	225	X:PVDF = 93:7	3.36, 2.1/3.51, 2.51	222/120	217/0.5 C/100	190/5 C	Cathode versus Na/Na^+	PTMA-impreg-nated CNT[69]
No. 60	491	218	X:vapor growth carbon fiber (VGCF):PVDF = 3:6:1	3.38/3.42	75/296	48.4/50 $mA\ g^{-1}$/50		Cathode versus Na/Na^+	[81]
No. 61	263	102	X:SWCNT = 9:1	3.5/3.5	93/80	56/1 C/200		Cathode versus Li/Li^+	[82]
No. 62	199	270	X:CB:PVDF = 7:2:1	3.56, 2.5–3.0/3.56, 2.5–3.0	261/	180/1 C/100	126/200 C	Cathode versus Li/Li^+	PTVE/graphene nanocomposite[71]
	199	270	X:CB:PVDF = 1:8:1		227/	120/1 C/100	52/200 C	Cathode versus Li/Li^+	[71]
No. 64	312	172	X:graphite:CB:PVDF = 20:34:7:39	3.0–4.2/	73/	65/1 C/500		Cathode versus Li/Li^+	[84]

Table 2 Continued.

A	B	C	D	E	F	G	H	I	J
No. 65	256	104	X:VGCF:PVDF = 1:8:1	3.66/	80/	72/10 C/100		Cathode versus Li/Li^+	[85]
No. 66	182	147	X:VGCF:PVDF = 1:8:1	3.7/	90/	72/10 C/1000		Cathode versus Li/Li^+	[66]
No. 69	173	620	X:CB:PVDF = 6:3:1	2.35, 1.9/2.1	560/153	131/0.5 C/100	50/20 C	Cathode versus Li/Li^+	[30]
No. 70	187	573	X:CB:PVDF = 6:3:1		310/67	34/0.5 C/50		Cathode versus Li/Li^+	[30]
No. 71	205	1830	X:AB:PVDF = 8:1:1	1.5/0.75, 1.6	928/383	1536/100 mA g^{-1}/500	217/5 C	Anode versus Li/Li^+	COF@CNTs composite[92]
	205	1830	X:AB:PVDF = 8:1:1			125/100 mA g^{-1}/300		Anode versus Li/Li^+	[92]
No. 72	915	176	X:CB:CMC = 7:2:1	2.5/3.0	230/	200/0.01 A g^{-1}/40	50/5 A g^{-1}	Cathode versus Na/Na^+	[98]
	915	176	X:CB:CMC = 7:2:1	1.5/1.6	38/		223/2 A g^{-1}	Cathode versus Na/Na^+	All organic batteries[99]
No. 73	1405	228	X:CNT:PVDF = 7:2:1	1.4/	2497/1319	1015/0.1 A g^{-1}/230	257/2.3 A g^{-1}	Anode versus Li/Li^+	NG-HCP nanosheets[93]
No. 74	1376	117	X:SP:sodium alginate = 8:1:1	2.4, 1.58/2.45, 1.60	62.5/			Cathode versus Li/Li^+	[94]
	1376	117	X:SP:sodium alginate = 8:1:1	2.4, 1.58/2.45, 1.60	116/	95/0.5 A g^{-1}/1000	94/1.0 A g^{-1}	Cathode versus Li/Li^+	2DCCP-HATN@CNT[94]
No. 75	1301	124	X:SP:sodium alginate = 8:1:1	2.4, 1.58/2.45, 1.60				Cathode versus Li/Li^+	[94]
No. 76	386	278	X:SP:sodium alginate = 6:3:1	1.4/1.5	315/	170/0.3 C/150	42/40 C	Cathode versus Na/Na^+	[95]
No. 77	966	111	X:SP:PVDF = 6:3:1	3.6,2.7/		115/0.16 C/3		Cathode versus Li/Li^+	[100]

One of the high LUMO levels indicates that the low-potential n-doping process is difficult. Obviously, the reduction potential of OCNs based on the same element site has an approximately negative linear relationship with the LUMO energy (Figure 13b–d). According to the LUMO level of the compounds that have not been applied in the batteries, it can be preliminarily known that the experimental reduction potential should be located near ★. Although the electrochemical activities are affected by factors such as the electrochemical system and manufacturing process of test batteries, the experimental errors are also inevitable, but the theoretical calculation results still have reference significance.

The difference between the LUMO diagrams can explain the performance difference of OCNs based on the same nitrogen-containing groups (Figure 13e). For C=N in chains, there is a clear difference between the LUMO diagrams of No. 2, which meets the Hückel rule, and No. 1 that does not, indicating that the active sites of No. 2 have the better electron-withdrawing ability. A lack of a benzene ring in the middle block of No. 6 distorts the molecule and reduces the electron-withdrawing ability of the active site. Although the LUMO levels of the abovementioned three molecules are similar, the electrochemical activity of No. 2 is higher than that of Nos. 1 and 6. This confirms the contribution of the Hückel active structure and benzene ring to the electrochemical activity of Schiff base compounds. For C=N in heteroaromatic compounds, the LUMO diagrams of No. 30 show that the active site has a good electron-withdrawing ability and electrochemical activity. Moreover, the nitrogen-containing aromatic heterocycle can reduce the LUMO level and increase the reduction potential,[111] so the potential of C=N in heteroaromatic molecules is higher overall than that of C=N in chains. The LUMO diagrams of No. 37 show that C≡N has a good electron-withdrawing ability and electr0chemical activity, so the reduction potential of C=N in heteroaromatic molecules is also higher than that of C=N in chains. The similar LUMO diagrams of the aromatic azo compounds represented by Nos. 43 and 46 indicate that the N=N connected to the benzene ring has good electrochemical activity and stability, while the conjugate of N=N in aliphatic azo compound No. 57 is reduced, resulting in electrochemical activity loss. Moreover, during the calculation process, it was found that the structures of Nos. 56 and 57 were unstable, and the structure of No. 58 was stable, which is consistent with the experimental results in the literature. The similar lower LUMO levels of nitroxyl radicals indicate that high-potential p-type doping reactions can be performed, which is consistent with the reported results. However, the large difference between the higher LUMO levels makes the nitroxyl radicals react differently in low-platform n-type doping, resulting in some nitroxyl radicals having a low-potential plateau and high capacity and some not having low-potential

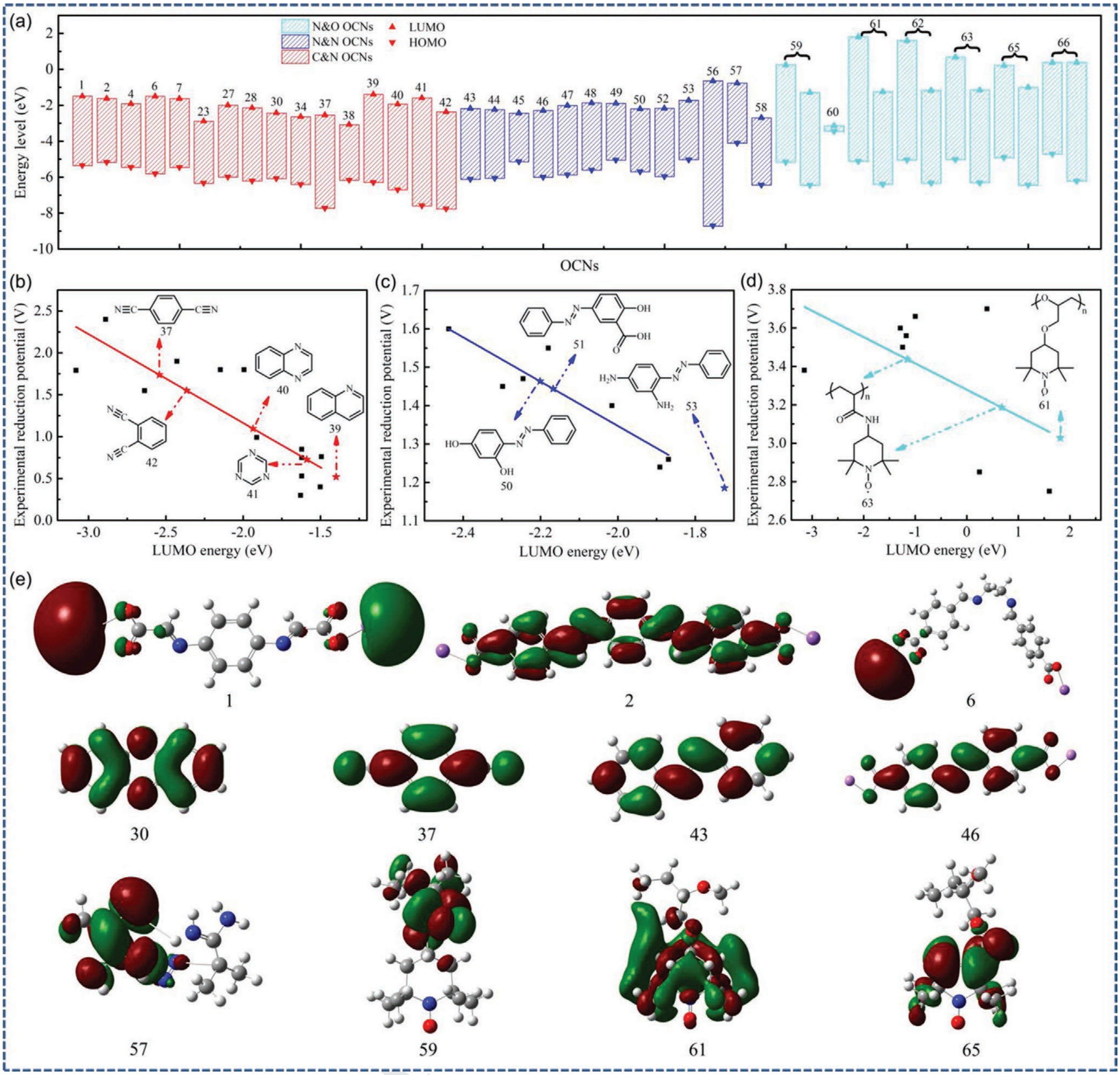

Figure 13. a) LUMO and HOMO levels of the selected compounds calculated by DFT, where the bars represent the energy gap. OCNs based on carbon–nitrogen groups (red), nitrogen–nitrogen groups (blue) and nitrogen–oxygen groups (light blue). Linear graphs of the experimental reduction potential and LUMO energy of OCNs based on b) carbon–nitrogen groups, c) nitrogen–nitrogen groups and d) nitrogen–oxygen groups. e) LUMO plots of some compounds in a). The lowest-energy geometry for each molecular model was determined in the gas phase by the Gaussian 16 package[1] with tight convergence criteria. The B3LYP hybrid functional (the Becke 3-parameter exchange functional combined with the Lee–Yang–Parr correlation functional) and the 6–31G** basis set were used in the calculations for all atoms. The frontier orbitals of each were computed using their optimized geometry and visualized in the GaussView 5.0 program.

n-doping reactions and low capacity. Therefore, the next step is to increase the capacity of nitroxyl radicals to their $C_{\text{theoretical}}$.

4.1.3. Analysis of COFs in OCNs

The COFs in OCNs can contain single nitrogen-containing groups. C≡N and nitroxyl radicals exist only in the end groups, and the specific gravity of the active site is small. The C=N and N=N groups in chains both have functions of providing an electrochemical activity and connecting the molecular skeleton, but the specific gravity of the active site is small. In addition to the aforementioned advantages, the highly conjugated C=N group in heteroaromatic molecules also has good electronic conductivity and provides more sites for each repeating unit. In addition, the adjustability of C=N can provide COFs with

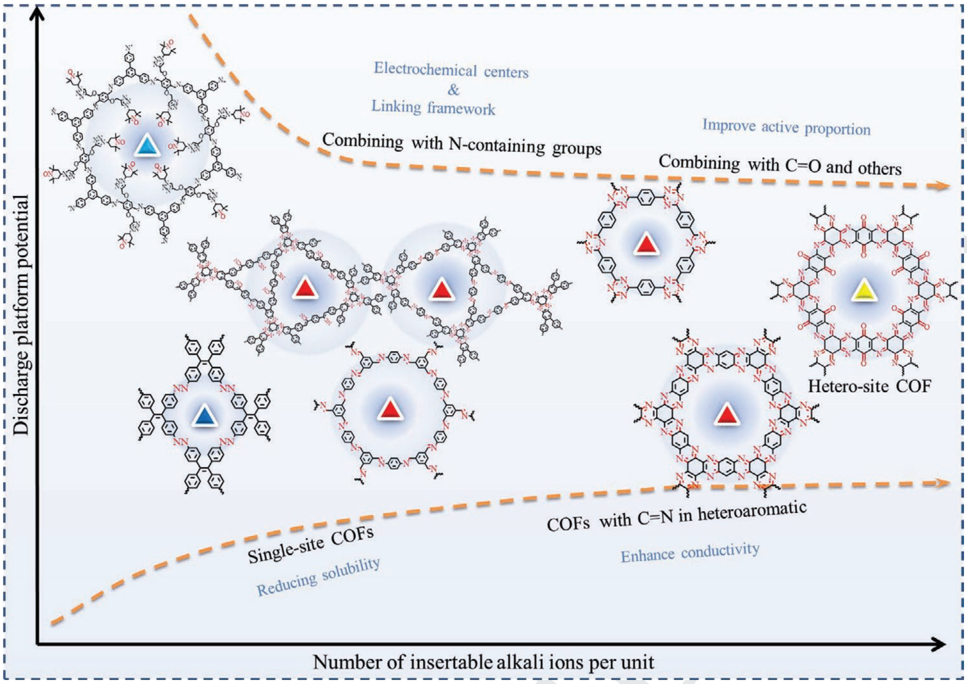

Figure 14. Strategies for improving the electrochemical performance of COFs in OCNs. The triangles represent the positions of OCNs. The red, blue and cyan triangles are based on carbon–nitrogen groups, nitrogen–nitrogen groups and nitrogen–oxygen groups, respectively. The yellow one is heterosite COF.

structural diversity and a high proportion of active parts. Therefore, the addition of C=N in heteroaromatic molecules in COFs is a good choice to improve the electrochemical performance. To solve the problems of the low electronic conductivity and high specific gravity of the inactive parts of single-site COFs, combining many active sites with highly conductive structures is a good strategy (**Figure 14**). The first approach is the combination of nitrogen-containing groups in COFs, such as No. 74. The second is the combination of nitrogen-containing groups and other active groups including C=O. For example, the combination of a highly conductive phenazine and a highly active C=O group has been shown to allow COFs to have both a high capacity and good rate performance.[103]

4.2. Electrochemical Contributions of N in OCNs

The roles of N in OCNs at different nitrogen sites have common points and differences. In this review, according to the overview of OCNs applied to alkali metal rechargeable batteries with organic electrolytes, the electrochemical contribution of N in OCNs can be shown as follows (**Figure 15**). 1) N provides electrochemical activity. N exists in the electrochemical active centers formed by the combination of C, N, and O, which provide the possibility of the insertion of alkali metal ions. 2) N provides more Li storage sites for the unit active site. 3) N extends the conjugate structure. N has 3 unpaired electrons, which can easily form p–π conjugates with the adjacent π bond to extend the conjugate structure; thus, the charge exchange between the molecule and lithium ion is facile, and the organic electrode has a rapid charge and discharge capability[28,47] 4) N provides stability. The nitrogen-containing groups have high stability during the redox process, the molecular structure is not easily destroyed, and the electrode has a good cycle stability. 5) N provides conductivity. In organic molecules, due to the three unpaired electrons in N and the electron-donating group containing N, the intrinsic conductivity of the organic molecule is improved, and so it exhibits

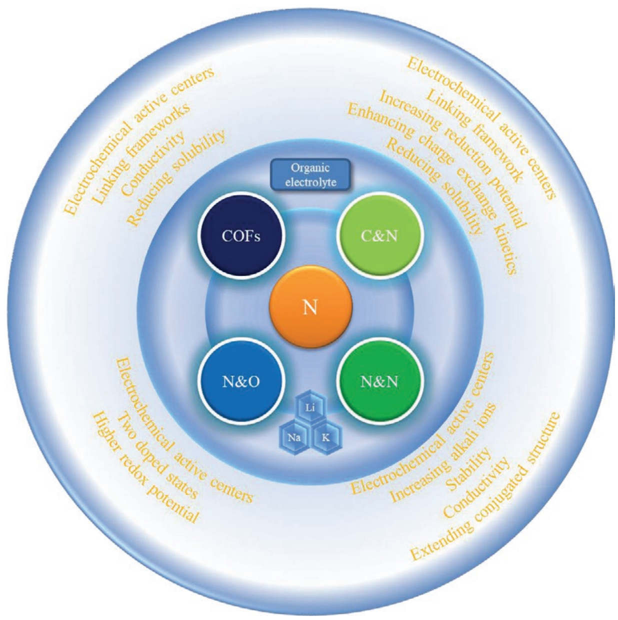

Figure 15. Electrochemical contributions of N in OCNs.

a good rate performance. 6) N increases the reduction potential. In heteroaromatic molecules, N has dual roles, acting as the active center and heteroaromatic N, providing electrochemical activity and increasing the reduction potential of the molecule. 7) As a part of the insoluble framework, alkali metal ions are stored, and the dissolution inertness increases simultaneously. In addition, N can also enhance charge exchange kinetics and provide two doping states. N in the inactive center can also affect the electrochemical activity of organic molecules. For example, N in the active center assists the carbonyl group to co-coordinate N and O to Li[49] and can increase the reduction potential of organic molecules in a heteroaromatic compound[26]

5. Conclusions and Outlook

5.1. Conclusions

In summary, OCNs have great application prospects in batteries due to their diversity and adjustability. The electrochemical activities of OCNs based on carbon–nitrogen groups with the special structure are improved. OCNs based on nitrogen–nitrogen groups provide many Li storage sites per unit active site. Nitroxyl radicals show rapid reaction kinetics and a high operating voltage. The nitrogen-containing groups in COFs are active centers and connect the molecular skeleton. Research on improving the performance of OCNs provides a potential choice for electrode material design. The electrochemical activity of OCNs based on different nitrogen-containing groups relies on the electronegativity of the constituent group elements, which is the main difference between the reduction or oxidation potentials. The electrochemical activity of OCNs based on the same nitrogen-containing group depends on the position of the group and the molecular structure. Among them, nitrogen-containing heteroaromatic molecules can exhibit good electrochemical activity and electronic conductivity. The roles of N in the active center of OCNs correspond to the specific composition and molecular structure of nitrogen-containing groups. The more tunable the nitrogen-containing group, the more important the role of N.

However, the high solubility and low electronic conductivity of OCNs are the primary problems we face, and long cycle life and high capacity density still need to be achieved. There is still a large gap between the current research states of OCNs and their commercial application. At the same time, there are two improvement measures to solve the problems of high solubility and low electronic conductivity. One is to optimize the molecules themselves. Small molecules can be prepared as corresponding alkali metal salts or extended conjugated structures, while the polymers inhibit dissolution by large molecular weight and conjugate skeletons and improve electronic conductivity by introducing N atoms. The other is combining insoluble conductive substrates by physical effects and stable chemical bonds, such as carbon fiber felt,[112] CNTs, MXene, graphene, CMK-3, etc. In addition to the exploration of substrate materials, the electrode fabrication process also merits further study. To further improve the electrochemical performance, the micro morphology design is also necessary.

5.2. Outlook

With the development of the following five aspects, the prospects of OCNs as organic electrode materials can be further improved. 1) Exploring more OCNs applied in alkali metal rechargeable batteries with organic/aqueous electrolytes is a long-term theme. 2) It is necessary to conduct in-depth study of the electrochemical reaction mechanism and characteristics of the charge/discharge process of OCNs. 3) Extensive research on LIBs, NIBs, and KIBs will provide a wider range of applications for OCNs. 4) The fabrications of new generation electrodes, such as self-standing electrode and flexible electrode, will open new windows. 5) Considering the development of solid electrolytes, the combination of organic electrode materials and solid electrolytes can simultaneously solve the dissolution problem and maintain long cycle life and high energy density. In addition, it is necessary to establish and improve the database information of the electrochemical active organic molecules that have been studied.

Finally, in regard to deeper future visions, the cost issue of OCNs deserves more attention. There are four ways to obtain low-cost and environmentally friendly organic materials: development of low-cost synthetic routes for OCNs and other organic materials, applications of natural electrochemical active organic materials in rechargeable batteries, recycling of electrochemical active organic materials in waste liquid, and industrial production of organic materials.

Acknowledgements

Q.Y. and Z.X. contributed equally to this work. The present work was funded by the Key Research and Development Program of Hubei, China (2020BHE013) and the Australian Research Council (No. CE140100003, DP180101581). The computational aspects of this work were supported by an award under the National Computational Merit Allocation Scheme (NCMAS) for JY of the National Computing Infrastructure (NCI) National Facility at Australian National University and Pawsey Supercomputing Centre in Western Australia.

Conflict of Interest

The authors declare no conflict of interest.

Keywords

covalent organic framework, electrochemical activity, electrode materials, nitrogen-containing group

Received: August 5, 2020
Revised: October 18, 2020
Published online:

[1] J.-M. Tarascon, *Phil. Trans. R. Soc. A* **2010**, *368*, 3227.
[2] C. Deng, Z. Wang, L. Feng, S. Wang, J. Yu, *J. Mater. Chem. A* **2020**, *8*, 19704.
[3] H. Rahimi-Eichi, U. Ojha, F. Baronti, M.-Y Chow, *IEEE Ind. Electron. Mag.* **2013**, *7*, 4.

[4] M. Li, J. Lu, Z. Chen, K. Amine, *Adv. Mater.* **2018**, *30*, 1800561.
[5] E. A. Olivetti, G. Ceder, G. G. Gaustad, X. Fu, *Joule* **2017**, *1*, 229.
[6] Y. Xu, X. Wang, Z. Wang, S. Wang, X. Zhu, D. Li, J. Yu, *Nanoscale* **2020**, *12*, 10205.
[7] Y. Chang, H. Zhang, W. Xiang, S. Wang, X. Zhu, J. Yu, *Electrochim. Acta* **2020**, *339*, 135918.
[8] M. Armand, J.-M. Tarascon, *Nature* **2008**, *451*, 652.
[9] B. Dunn, H. Kamath, J.-M. Tarascon, *Science* **2011**, *334*, 928.
[10] F.-C. Chang, Y.-C. Li, R.-J. Wu, C.-H. Chen, *ACS Appl. Nano Mater.* **2019**, *2*, 2515.
[11] K. Zhang, Z. Hu, Z. Tao, J. Chen, *Sci. China Mater.* **2014**, *57*, 42.
[12] S. Wang, L. Wang, Z. Zhu, Z. Hu, Q. Zhao, J. Chen, *Angew. Chem., Int. Ed.* **2014**, *53*, 5892.
[13] Q. Zhao, Y. Lu, J. Chen, *Adv. Energy Mater.* **2017**, *7*, 1601792.
[14] K. Lei, F. Li, C. Mu, J. Wang, Q. Zhao, C. Chen, J. Chen, *Energy Environ. Sci.* **2017**, *10*, 552.
[15] J. B. Goodenough, Y. Kim, *Chem. Mater.* **2010**, *22*, 587.
[16] M. S Whittingham, *Chem. Rev.* **2014**, *114*, 11414.
[17] F. Cheng, J. Liang, Z. Tao, J. Chen, *Adv. Mater.* **2011**, *23*, 1695.
[18] Y. Lu, J. Chen, *Nat. Rev. Chem.* **2020**, *4*, 127.
[19] Y. Liang, Z. Tao, J. Chen, *Adv. Energy Mater.* **2012**, *2*, 742.
[20] P. Poizot, F. Dolhem, *Energy Environ. Sci.* **2011**, *4*, 2003.
[21] Y. Lu, Q. Zhang, J. Chen, *Sci. China Chem.* **2019**, *62*, 533.
[22] Q. Zhao, C. Guo, Y. Lu, L. Liu, J. Liang, J. Chen, *Ind. Eng. Chem. Res.* **2016**, *55*, 5795.
[23] J. Kim, J. H. Kim, K. Ariga, *Joule* **2017**, *1*, 739.
[24] M. Wu, Y. Cui, A. Bhargav, Y. Losovyj, A. Siegel, M. Agarwal, Y. Ma, Y. Fu, *Angew. Chem., Int. Ed.* **2016**, *55*, 10027.
[25] K. Nakahara, S. Iwasa, M. Satoh, Y. Morioka, J. Iriyama, M. Suguro, E. Hasegawa, *Chem. Phys. Lett.* **2002**, *359*, 351.
[26] Q. Zhao, Z. Zhu, J. Chen, *Adv. Mater.* **2017**, *29*, 1607007.
[27] Y. Lu, Q. Zhang, L. Li, Z. Niu, J. Chen, *Chem* **2018**, *4*, 2786.
[28] C. Luo, O. Borodin, X. Ji, S. Hou, K. J. Gaskell, X. Fan, J. Chen, T. Deng, R. Wang, J. Jiang, C. Wang, *Proc. Natl. Acad. Sci. USA* **2018**, *115*, 2004.
[29] C. Luo, G.-L. Xu, X. Ji, S. Hou, L. Chen, F. Wang, J. Jiang, Z. Chen, Y. Ren, K. Amine, C. Wang, *Angew. Chem., Int. Ed.* **2018**, *57*, 2879.
[30] C. Luo, X. Ji, S. Hou, N. Eidson, X. Fan, Y. Liang, T. Deng, J. Jiang, C. Wang, *Adv. Mater.* **2018**, *30*, 1706498.
[31] Y. Liang, C. Luo, F. Wang, S. Hou, S.-C Liou, T. Qing, Q. Li, J. Zheng, C. Cui, C. Wang, *Adv. Energy Mater.* **2019**, *9*, 1802986.
[32] J. Xie, X. Rui, P. Gu, J. Wu, Z. J. Xu, Q. Yan, Q. Zhang, *ACS Appl. Mater. Interfaces* **2016**, *8*, 16932.
[33] S. Renault, V. A. Oltean, C. M Araujo, A. Grigoriev, K. Edström, D. Brandell, *Chem. Mater.* **2016**, *28*, 1920.
[34] B. Häupler, A. Wild, U. S. Schubert, *Adv. Energy Mater.* **2015**, *5*, 1402034.
[35] E. Castillo-Martínez, J. Carretero-González, M. Armand, *Angew. Chem., Int. Ed.* **2014**, *53*, 5341.
[36] M. López-Herraiz, E. Castillo-Martínez, J. Carretero-González, J. Carrasco, T. Rojo, M. Armand, *Energy Environ. Sci.* **2015**, *8*, 3233.
[37] X. Yin, S. Sarkar, S. Shi, Q. A. Huang, H. Zhao, L. Yan, Y. Zhao, J. Zhang, *Adv. Funct. Mater.* **2020**, *30*, 1908445.
[38] N. Fernández, P. Sánchez-Fontecoba, E. Castillo-Martínez, J. Carretero-González, T. Rojo, M. Armand, *ChemSusChem* **2018**, *11*, 311.
[39] Z. Man, P. Li, D. Zhou, R. Zang, S. Wang, P. Li, S. Liu, X. Li, Y. Wu, X. Liang, G. Wang, *J. Mater. Chem. A* **2019**, *7*, 2368.
[40] H. Ye, F. Jiang, H. Li, Z. Xu, J. Yin, H. Zhu, *Electrochim. Acta* **2017**, *253*, 319.
[41] Y. Sun, Y. Sun, Q. Pan, G. Li, B. Han, D. Zeng, Y. Zhang, H. Cheng, *Chem. Commun.* **2016**, *52*, 3000.
[42] B. Lee, Y. Ko, G. Kwon, S. Lee, K. Ku, J. Kim, K. Kang, *Joule* **2018**, *2*, 61.
[43] M. Lee, J. Hong, D.-H. Seo, D. H. Nam, K. T Nam, K. Kang, C. B. Park, *Angew. Chem., Int. Ed.* **2013**, *52*, 8322.
[44] M. Lee, J. Hong, H. Kim, H.-D. Lim, S. B. Cho, K. Kang, C. B. Park, *Adv. Mater.* **2014**, *26*, 2558.
[45] J. Hong, M. Lee, B. Lee, D.-H. Seo, C. B. Park, K. Kang, *Nat. Commun.* **2014**, *5*, 5335.
[46] B. Tian, Z. Ding, G.-H. Ning, W. Tang, C. Peng, B. Liu, J. Su, C. Su, K. P. Loh, *Chem. Commun.* **2017**, *53*, 2914.
[47] C. Peng, G.-H. Ning, J. Su, G. Zhong, W. Tang, B. Tian, C. Su, D. Yu, L. Zu, J. Yang, M.-F. Ng, Y.-S. Hu, Y. Yang, M. Armand, K. P. Loh, *Nat. Energy* **2017**, *2*, 17074.
[48] Q. Deng, S.-J. He, J. Pei, C. Fan, C. Li, B. Cao, Z.-H. Lu, J. Li, *Electrochem. Commun.* **2017**, *75*, 29.
[49] A. Shimizu, Y. Tsujii, H. Kuramoto, T. Nokami, Y. Inatomi, N. Hojo, J.-I. Yoshida, *Energy Technol.* **2014**, *2*, 155.
[50] B. V. Ratnakumar, S. Di Stefano, R. M. Williams, G. Nagasubramanian, C. P. Bankston, *J. Appl. Electrochem.* **1990**, *20*, 357.
[51] Y. Chen, S. Manzhos, *Mater. Chem. Phys.* **2015**, *156*, 180.
[52] Y. Chen, S. Manzhos, *Phys. Chem. Chem. Phys.* **2016**, *18*, 8874.
[53] R. Precht, R. Hausbrand, W. Jaegermann, *Phys. Chem. Chem. Phys.* **2015**, *17*, 6588.
[54] R. Precht, S. Stolz, E. Mankel, T. Mayer, W. Jaegermann, R. Hausbrand, *Phys. Chem. Chem. Phys.* **2016**, *18*, 3056.
[55] Y. Hanyu, I. Honma, *Sci. Rep.* **2012**, *2*, 453.
[56] K. H Jung, G. S. Jeong, C. Y. Go, K. C Kim, *Energy Storage Mater.* **2020**, *24*, 237.
[57] C. Cui, X. Ji, P.-F. Wang, G.-L. Xu, L. Chen, J. Chen, H. Kim, Y. Ren, F. Chen, C. Yang, X. Fan, C. Luo, K. Amine, C. Wang, *ACS Energy Lett.* **2020**, *5*, 224.
[58] Q. Zhao, A. Whittaker, X. Zhao, *Materials* **2018**, *11*, 2567.
[59] H. Peng, Q. Yu, S. Wang, J. Kim, A. E. Rowan, A. K. Nanjundan, Y. Yamauchi, J. Yu, *Adv. Sci.* **2019**, *6*, 1900431.
[60] C. Luo, X. Ji, J. Chen, K. J. Gaskell, X. He, Y. Liang, J. Jiang, C. Wang, *Angew. Chem., Int. Ed.* **2018**, *57*, 8567.
[61] C. Luo, R. Huang, R. Kevorkyants, M. Pavanello, H. He, C. Wang, *Nano Lett.* **2014**, *14*, 1596.
[62] M. Armand, S. Grugeon, H. Vezin, S. Laruelle, P. Ribière, P. Poizot, J.-M. Tarascon, *Nat. Mater.* **2009**, *8*, 120.
[63] Q. Deng, J. Pei, C. Fan, J. Ma, B. Cao, C. Li, Y. Jin, L. Wang, J. Li, *Nano Energy* **2017**, *33*, 350.
[64] J. C. Pramudita, D. Sehrawat, D. Goonetilleke, N. Sharma, *Adv. Energy Mater.* **2017**, *7*, 1602911.
[65] Y. Zhu, P. Chen, Y. Zhou, W. Nie, Y. Xu, *Electrochim. Acta* **2019**, *318*, 262.
[66] K. Oyaizu, T. Kawamoto, T. Suga, H. Nishide, *Macromolecules* **2010**, *43*, 10382.
[67] S. Muench, A. Wild, C. Friebe, B. Häupler, T. Janoschka, U. S. Schubert, *Chem. Rev.* **2016**, *116*, 9438.
[68] K. Oyaizu, H. Nishide, *Adv. Mater.* **2009**, *21*, 2339.
[69] J.-K. Kim, Y. Kim, S. Park, H. Ko, Y. Kim, *Energy Environ. Sci.* **2016**, *9*, 1264.
[70] W. Guo, Y.-X Yin, S. Xin, Y.-G Guo, L.-J Wan, *Energy Environ. Sci.* **2012**, *5*, 5221.
[71] W. Guo, J. Su, Y.-H. Li, L.-J Wan, Y.-G. Guo, *Electrochim. Acta* **2012**, *72*, 81.
[72] K. Zhang, Y. Hu, L. Wang, J. Fan, M. J. Monteiro, Z. Jia, *Polym. Chem.* **2017**, *8*, 1815.
[73] Y. Yonekuta, K. Oyaizu, H. Nishide, *Chem. Lett.* **2007**, *36*, 866.
[74] K. Nakahara, J. Iriyama, S. Iwasa, M. Suguro, M. Satoh, E. J. Cairns, *J. Power Sources* **2007**, *165*, 398.
[75] K. Nakahara, J. Iriyama, S. Iwasa, M. Suguro, M. Satoh, E. J. Cairns, *J. Power Sources* **2007**, *165*, 870.
[76] C.-H. Lin, J.-T. Lee, D.-R. Yang, H.-W. Chen, S.-T. Wu, *RSC Adv.* **2015**, *5*, 33044.
[77] K. Oyaizu, Y. Ando, H. Konishi, H. Nishide, *J. Am. Chem. Soc.* **2008**, *130*, 14459.

[78] T. Katsumata, J. Qu, M. Shiotsuki, M. Satoh, J. Wada, J. Igarashi, K. Mizoguchi, T. Masuda, *Macromolecules* **2008**, *41*, 1175.
[79] Y. Dai, Y. Zhang, L. Gao, G. Xu, J. Xie, *J. Electrochem. Soc.* **2011**, *158*, A291.
[80] T. Suga, H. Ohshiro, S. Sugita, K. Oyaizu, H. Nishide, *Adv. Mater.* **2009**, *21*, 1627.
[81] Y. Dai, Y. Zhang, L. Gao, G. Xu, J. Xie, *Electrochem. Solid-State Lett.* **2010**, *13*, A22.
[82] T. Sukegawa, K. Sato, K. Oyaizu, H. Nishide, *RSC Adv.* **2015**, *5*, 15448.
[83] N. Sano, W. Tomita, S. Hara, C.-M. Min, J.-S. Lee, K. Oyaizu, H. Nishide, *ACS Appl. Mater. Interfaces* **2013**, *5*, 1355.
[84] P. Nesvadba, L. Bugnon, P. Maire, P. Novák, *Chem. Mater.* **2010**, *22*, 783.
[85] K. Oyaizu, T. Suga, K. Yoshimura, H. Nishide, *Macromolecules* **2008**, *41*, 6646.
[86] T. Suga, S. Sugita, H. Ohshiro, K. Oyaizu, H. Nishide, *Adv. Mater.* **2011**, *23*, 751.
[87] T. Suga, Y.-J. Pu, S. Kasatori, H. Nishide, *Macromolecules* **2007**, *40*, 3167.
[88] A. Molina, N. Patil, E. Ventosa, M. Liras, J. Palma, R. Marcilla, *Adv. Funct. Mater.* **2020**, *30*, 1908074.
[89] K. Amin, L. Mao, Z. Wei, *Macromol. Rapid Commun.* **2019**, *40*, 1800565.
[90] F. Beuerle, B. Gole, *Angew. Chem., Int. Ed.* **2018**, *57*, 4850.
[91] T. Sun, J. Xie, W. Guo, D. S. Li, Q. Zhang, *Adv. Energy Mater.* **2020**, *10*, 1904199.
[92] Z. Lei, Q. Yang, Y. Xu, S. Guo, W. Sun, H. Liu, L.-P Lv, Y. Zhang, Y. Wang, *Nat. Commun.* **2018**, *9*, 576.
[93] Z.-Q. Lin, J. Xie, B.-W. Zhang, J.-W. Li, J. Weng, R.-B. Song, X. Huang, H. Zhang, H. Li, Y. Liu, Z. J. Xu, W. Huang, Q. Zhang, *Nano Energy* **2017**, *41*, 117.
[94] S. Xu, G. Wang, B. P. Biswal, M. Addicoat, S. Paasch, W. Sheng, X. Zhuang, E. Brunner, T. Heine, R. Berger, X. Feng, *Angew. Chem., Int. Ed.* **2019**, *58*, 849.
[95] K. S Weeraratne, A. A. Alzharani, H. M. El-Kaderi, *ACS Appl. Mater. Interfaces* **2019**, *11*, 23520.
[96] S. Kandambeth, K. Dey, R. Banerjee, *J. Am. Chem. Soc.* **2019**, *141*, 1807.
[97] K. Sakaushi, G. Nickerl, F. M. Wisser, D. Nishio-Hamane, E. Hosono, H. Zhou, S. Kaskel, J. Eckert, *Angew. Chem., Int. Ed.* **2012**, *51*, 7850.
[98] K. Sakaushi, E. Hosono, G. Nickerl, T. Gemming, H. Zhou, S. Kaskel, J. Eckert, *Nat. Commun.* **2013**, *4*, 1485.
[99] K. Sakaushi, E. Hosono, G. Nickerl, H. Zhou, S. Kaskel, J. Eckert, *J. Power Sources* **2014**, *245*, 553.
[100] S. Wang, Q. Wang, P. Shao, Y. Han, X. Gao, L. Ma, S. Yuan, X. Ma, J. Zhou, X. Feng, B. Wang, *J. Am. Chem. Soc.* **2017**, *139*, 4258.
[101] G. Wang, N. Chandrasekhar, B. P. Biswal, D. Becker, S. Paasch, E. Brunner, M. Addicoat, M. Yu, R. Berger, X. Feng, *Adv. Mater.* **2019**, *31*, 1901478.
[102] S. Gu, S. Wu, L. Cao, M. Li, N. Qin, J. Zhu, Z. Wang, Y. Li, Z. Li, J. Chen, Z. Lu, *J. Am. Chem. Soc.* **2019**, *141*, 9623.
[103] E. Vitaku, C. N. Gannett, K. L. Carpenter, L. Shen, H. D. Abruña, W. R. Dichtel, *J. Am. Chem. Soc.* **2020**, *142*, 16.
[104] R. Shi, L. Liu, Y. Lu, C. Wang, Y. Li, L. Li, Z. Yan, J. Chen, *Nat. Commun.* **2020**, *11*, 178.
[105] J. Guo, Y. Xu, S. Jin, L. Chen, T. Kaji, Y. Honsho, M. A. Addicoat, J. Kim, A. Saeki, H. Ihee, S. Seki, S. Irle, M. Hiramoto, J. Gao, D. Jiang, *Nat. Commun.* **2013**, *4*, 2736.
[106] S. Dalapati, S. Jin, J. Gao, Y. Xu, A. Nagai, D. Jiang, *J. Am. Chem. Soc.* **2013**, *135*, 17310.
[107] K. Dey, M. Pal, K. C. Rout, S. Kunjattu H, A. Das, R. Mukherjee, U. K. Kharul, R. Banerjee, *J. Am. Chem. Soc.* **2017**, *139*, 13083.
[108] P. J. Waller, S. J. Lyle, T. M. Osborn Popp, C. S. Diercks, J. A. Reimer, O. M. Yaghi, *J. Am. Chem. Soc.* **2016**, *138*, 15519.
[109] R. Zhao, Z. Liang, R. Zou, Q. Xu, *Joule* **2018**, *2*, 2235.
[110] Z. Zhang, H. Yoshikawa, K. Awaga, *J. Am. Chem. Soc.* **2014**, *136*, 16112.
[111] L.-B. Zhao, S.-T. Gao, R. He, W. Shen, M. Li, *ChemSusChem* **2018**, *11*, 1215.
[112] H. Peng, P. Chen, X. Yang, Z. Xue, S. Wang, J. Na, J. Yu, Y. Yamauchi, *J. Mater. Chem. A* **2020**, *8*, 11521.

Qianchuan Yu is currently studying for his M.Sc. degree at the Faculty of Materials Science and Chemistry, China University of Geosciences (Wuhan). He received his B.Sc. degree in chemical engineering from Shihezi University, China. His current research is focused on the application of organic electrode materials.

Zhihuan Xue is currently studying for her M.Sc. degree at the Faculty of Materials Science and Chemistry, China University of Geosciences (Wuhan). She received her B.Sc. degree in applied chemistry from China University of Geosciences (Wuhan). Her current research focuses on the organic molecules as electrode materials in lithium batteries.

Shengping Wang is a Professor in the Department of Chemistry, China University of Geosciences. Before becoming a professor, he worked in a factory of lithium batteries for 8 years. He has devoted himself to the study of secondary and primary lithium batteries for 20 years, such as Li/MnO_2 batteries, $Li/SOCl_2$ batteries, Li/S batteries, and lithium (sodium, zinc) ion batteries.

Jingxian Yu received his Ph.D. in nanoscience and nanotechnology from Flinders University, Australia. He worked as a Roger Pysden Research Fellow at the University of Cambridge, and later at the University of Nottingham, U.K., as a postdoctoral research fellow. He returned to Australia in 2009 to take up an ARC Australian Postdoctoral Fellowship at the University of Adelaide, where he is currently a Senior Research Fellow & Senior Lecturer at the ARC Centre of Excellence for Nanoscale BioPhotonics (CNBP). His research interests focus on bio-inspired molecular electronics and nanomaterials for energy storage and biological applications.

Yusuke Yamauchi received his Ph.D. degree from Waseda University (2007), Japan. After that, he joined NIMS to start his own group. From 2017, he joined the University of Queensland (Australia) as a full-time professor. He concurrently serves as an honorary group leader in NIMS, a visiting professor at many universities in the world, and an associate editor of the Journal of Materials Chemistry A and Chemical Engineering Journal. His expertise is inorganic nanoarchitectonics, and has published more than 750 papers with >38 000 citations (h-index >100). He is selected as one of the Highly-Cited Researchers in Chemistry in 2016–2019.

ADVANCED ENERGY MATERIALS

Please complete this form and return it via E-Mail to the Editorial Office:
advenergymat@wiley-vch.de

Reprint Order Form

Manuscript No.: ________________________________

Customer No.: (if available) ________________________

Purchase Order No.: ________________________

Author: ________________________________

Charges for Reprints in Euro (excl. VAT), prices are subject to change. Minimum order 50 copies.

No. of pages	50 copies	100 copies	150 copies	200 copies	300 copies	500 copies
1– 4	345,—	395,—	425,—	445,—	548,—	752,—
5– 8	490,—	573,—	608,—	636,—	784,—	1077,—
9–12	640,—	739,—	786,—	824,—	1016,—	1396,—
13–16	780,—	900,—	958,—	1004,—	1237,—	1701,—
17–20	930,—	1070,—	1138,—	1196,—	1489,—	2022,—
every additional 4 pages	147,—	169,—	175,—	188,—	231,—	315,—

Information regarding VAT: The charges for publication of *reprints/poster* are considered to be "supply of services" and therefore subject to German VAT. However, if you are an institutional customer outside Germany, the tax can be waived if you provide us with the valid VAT number of your company. Non-EU customers may have a VAT number starting with "EU" instead of their country code, if they are registered with the EU tax authorities. If you do not have a valid EU VAT number and you are a taxable person doing business in a non-EU country, please provide a certification from your local tax authorities confirming that you are a taxable person under local tax law. Please note that the certification must confirm that you are a taxable person and are conducting an economic activity in your country. **Note:** certifications confirming that you are a tax-exempt legal body (non-profit organization, public body, school, political party, etc.) in your country do not exempt you from paying German VAT.

Please send me send bill me for

☐ no. of reprints

☐ high-resolution PDF file (330 Euro excl. VAT)
E-mail address: ____________________

❖ Special Offer:

If you order 200 or more reprints you will get a PDF file for half price.

Please note: It is not permitted to present the PDF file on the internet or on company homepages.

Cover Posters (prices excl. VAT)
Posters of published covers are available in two sizes:

☐ DIN A2 42 x 60 cm / 17 x 24in (one copy: 39 Euro)

☐ DIN A1 60 x 84 cm / 24 x 33in (one copy: 49 Euro)

Postage for shipping (prices excl. VAT)
overseas +25 Euro
within Europe +15 Euro

VAT number: ____________________________

Mail reprints / copies of the issue to:

____
____
____
____
____

Send bill to:

____
____
____
____

☐ **I will pay by bank transfer**

☐ **I will pay by credit card**

VISA, Mastercard and AMERICAN EXPRESS
For your security please use this link (Credit Card Token Generator) to create a secure code Credit Card Token and include this number in the form instead of the credit card data. Click here:
https://www.wiley-vch.de/editorial_production/index.php

CREDIT CARD TOKEN NUMBER

						V									

____
Date, Signature

Wiley-VCH GmbH – A company of John Wiley & Sons, Inc. -
Location of the Company: Weinheim - Trade Register: Mannheim, HRB 736569
Managing Directors: Sabine Haag und Guido Herrmann

WILEY-VCH